J. Fluid Mech. (1996), *vol.* 323, *pp.* 285–315

Minimum induced power requirements for flapping flight

By KENNETH C. HALL[1] AND STEVEN R. HALL[2]

[1]Department of Mechanical Engineering and Materials Science, Duke University, Durham, NC 27708-0300, USA

[2]Department of Aeronautics and Astronautics, Massachusetts Institute of Technology, Cambridge, MA 02139–4307, USA

(Received 21 October 1994 and in revised form 3 May 1996)

The Betz criterion for minimum induced loss is used to compute the optimal circulation distribution along the span of flapping wings in fast forward flight. In particular, we consider the case where flapping motion is used to generate both lift (weight support) and thrust. The Betz criterion is used to develop two different numerical models of flapping. In the first model, which applies to small-amplitude harmonic flapping motions, the optimality condition is reduced to a one-dimensional integral equation which we solve numerically. In the second model, which applies to large-amplitude periodic flapping motions, the optimal circulation problem is reduced to solving for the flow over an infinitely long wavy sheet translating through an inviscid fluid at rest at infinity. This three-dimensional flow problem is solved using a vortex-lattice technique. Both methods predict that the induced power required to produce thrust decreases with increasing flapping amplitude and frequency. Using the large-amplitude theory, we find that the induced power required to produce lift increases with flapping amplitude and frequency. Therefore, an optimum flapping amplitude exists when the flapping motion of wings must simultaneously produce lift and thrust.

1. Introduction

Wing flapping is a highly efficient means of propulsion. For example, using a quasi-steady theory, Betteridge & Archer (1974) have estimated that a sea gull (with weight W of 7.95 N, wing span b of 1.06 m, flight velocity U of 9.13 $\mathrm{m\,s^{-1}}$, and flapping frequency ω of 25.1 $\mathrm{rad\,s^{-1}}$) can achieve a maximum inviscid propulsive efficiency of 89.6%. Nevertheless, the fluid mechanics of flapping are not fully understood. For example, it is well known that to produce thrust the circulation should be greater on the downstroke than on the upstroke (at least for rigid wings flapping about a common hinge point on the longitudinal axis). It is not known, however, how to distribute the unsteady circulation along the span and over the flapping cycle to achieve a desired thrust and lift (weight support) and at the same time minimize the power required to flap the wings at realistic flapping frequencies and amplitudes.

Numerous experimental studies of flapping birds and bats have been reported in the literature. In particular Spedding, Rayner & Pennycuick (1984), Rayner, Jones & Thomas (1986), Spedding (1986, 1987), and Rayner (1991) have visualized the flow in the wakes behind birds and bats in flight. In these studies, the air in a laboratory

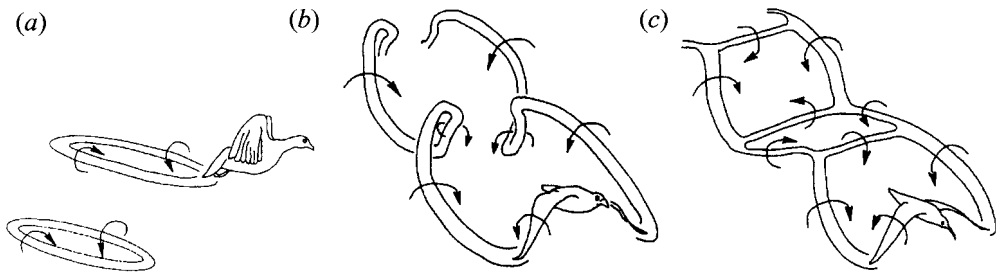

FIGURE 1. (*a*) Vortex-ring wake. (*b*) Concertina or continuous-vortex wake. (*c*) Ladder wake. Sketches after Pennycuick (1988).

was seeded with neutrally buoyant soap bubbles filled with helium. Trained birds and bats then flew through the seeded air, and the resulting flow structure in the wake of the animals was captured on film using stroboscopic photography. Rayner (1991) surveyed the available experimental data, and found that the structure of the wakes behind birds and bats falls into one of two distinct patterns. In slow flight, the wake appears to be composed of a series of vortex rings, one ring for each downstroke of the wings (see figure 1). In fast flight, the wake is composed of two undulating vortices which trail behind the animal. Furthermore, no transverse vorticity is observed. Quoting Rayner, "The absence of transverse vortices is not surprising, since the interaction of transverse vortices with the vortex on the wing can dramatically increase induced drag."

Based on these experimental observations, Rayner (1991, 1993) has proposed that birds use two distinct gaits: the vortex-ring gait and the continuous-wake gait. The vortex-ring gait is used in slow flight. According to Rayner, during the upstroke, the wing is flexed so that the span of the wing is reduced. Furthermore, the wing is aerodynamically inactive (little or no circulation is generated along the span of the wing). During the downstroke, the wing is fully extended and nearly flat, and the wing circulation along the span of the wing generates thrust and lift. The continuous-wake gait, on the other hand, is used in fast flight. The wing is aerodynamically active during both the downstroke and the upstroke with constant total circulation. During the downstroke, the wing is fully extended. During the upstroke, however, the wing is flexed or swept slightly to shorten the span of the wing, reducing the instantaneous lift while maintaining constant circulation.

Rayner (1991) has asserted that all vertebrates use one of these two gaits in forward flight. Although not yet experimentally observed in vertebrates, Pennycuick (1988) has speculated that humming birds use a third gait which generates a 'ladder wake' (see figure 1). Using this gait, the wings remain flat on both the upstroke and downstroke. The circulation is slightly larger on the downstroke than on the upstroke, generating thrust and depositing shed vorticity into the wake at the top and bottom of the stroke ('transverse vorticity' in the parlance of avian aerodynamicists).

While providing significant insight into the physics of flapping flight, flow visualization experiments have certain significant limitations. The wake rolls up rapidly behind the bird making it difficult to infer from measurements of the wake the precise history and distribution of circulation on the wing. The same can be said of fixed-wing aerodynamics. An elliptical circulation distribution along a fixed wing produces a continuous sheet of trailing vorticity behind the wing that rolls up into two tight trailing vortices with finite cores. The fact that the wake is composed of two discrete

trailing vortices, on the other hand, does not allow one to infer the precise circulation distribution on the wing. Nevertheless, the experimental observations of wakes behind birds and bats are invaluable for measuring the momentum and energy deposited in the wake, and for giving a general picture of the unsteady circulation distribution. Theoretical models of the aerodynamics of flapping, however, are required to fully understand flapping flight.

Using the experimental evidence of the vortex-ring structure of the wake behind birds in slow flight, Rayner (1979) has proposed a theory of bird flight whereby the wake of a flapping bird in forward flight is modelled as a sequence of elliptically shaped vortex rings. The spacing of the vortex rings was derived from the frequency of the flapping motion; the strength of the vortex rings and their orientation were chosen so as to produce the required thrust and lift. Finally, the induced power is simply the rate at which kinetic energy is deposited into the wake. However, since the kinetic energy of an ideal vortex ring is infinite, Rayner assumed that each vortex ring had a finite core radius. The size of the core radius was chosen based on correlations to fixed-wing models. Using a finite core radius, the resulting induced power is finite. Rayner's model – while perhaps qualitatively correct – suffers from a lack of knowledge of the unsteady circulation history. Furthermore, the proposed circulation distribution is impulsively started and stopped to form the vortex rings. Such an abrupt generation of circulation is unlikely to be optimum.

A number of investigators have studied the problem of flapping flight by modelling the flow field induced near the flapping wings due to the system of trailing and shed vorticity in the wake. For instance, Willmott (1988) developed an unsteady lifting-line theory using the method of matched asymptotic expansions for the general motion of a wing with high aspect ratio. The analysis was somewhat incomplete, however, in that the theory predicted the unsteady downwash at the trailing edge of the wing and some of the unsteady forces, but did not predict the induced drag. Phlips, East & Pratt (1981) modelled flapping using an unsteady lifting-line theory in which the shed or transverse vorticity in the wake was lumped at the start of each stroke. Ahmadi & Widnall (1985) developed an unsteady lifting-line theory using matched asymptotic expansions, with the inverse of the aspect ratio being the small parameter. Lan (1979) has developed an unsteady quasi-vortex-lattice method which he then applied to predict the flapping efficiency of various planforms and flapping motions, including the flapping of the tandem wings of dragonflies. All of these theories, however, are restricted to low-frequency flapping, i.e. the reduced frequency $k = \omega b/U \ll 1$ where ω is the flapping frequency, b is the wing span, and U is the flight speed. (Note that in the present definition of the reduced frequency, the wing span has been used as the characteristic length. Although other length scales, such as wing chord, could have been used, the span is most appropriate for the inviscid analysis since thrust, lift, and induced power depend on the spanwise loading, and not directly on the planform of the wing.)

The above analyses, while providing important understanding of the physics of flapping flight, give predictions of the energetics of flight for a prescribed wing motion. These theories do not address the question of optimum flight performance. Ahmadi & Widnall (1986) used their unsteady low-frequency lifting-line theory (Ahmadi & Widnall 1985) to compute the energetics of flapping motion of a rigid wing. The wing was assumed to oscillate with a combination of pitching and plunging motion. For a given wing planform and flapping frequency, they were able to calculate the combination of pitching and plunging motion that generated the desired thrust with minimum induced power. However, because the wing was assumed to be rigid,

the 'minimum' induced power found using this approach is larger than would be required if the pitching and plunging motion were allowed to vary along the span of the wing. In principle, however, the analysis of Ahmadi & Widnall (1986) could be extended to analyse this situation.

Instead of considering what wing motions produce a given thrust with minimum induced power, one might instead determine for a given flapping motion what unsteady circulation distribution is optimum, thus bypassing the difficult problem of computing the details of the flow in the near field of the wing. Betteridge & Archer (1974), using a combination of quasi-steady lifting-line theory and actuator-disk theory, considered very low-frequency flapping ($k \ll 1$) of high-aspect-ratio wings for the case where the left and right wings flap symmetrically about a common hinge point on the longitudinal axis. They decomposed the unsteady circulation along the span of the wing into a two-term Fourier series. Betteridge & Archer concluded (incorrectly) that the maximum propulsive efficiency is achieved when the unsteady incremental circulation distribution (that portion of the circulation which contributes to thrust) is elliptical in the spanwise direction. Jones (1980) considered the same problem posed by Betteridge & Archer and showed that the optimum circulation distribution for low-frequency small-amplitude flapping motion of high-aspect-ratio wings is not elliptical. Rather, the incremental circulation distribution is fuller near the tips than at the mid-span. Jones also showed that the optimum circulation distribution produces the same thrust for about 10% less power than an elliptical distribution.

The theories of Betteridge & Archer (1974) and Jones (1980) are restricted to very low-frequency small-amplitude motions. Notwithstanding these assumptions, their results predict that high induced propulsive efficiencies are achieved using flapping motions with large amplitudes and/or high frequencies. In fact, birds in fast forward flight are observed to flap their wings with moderately large frequencies. For example, Tucker (1968, 1973) studied the flight of budgerigars (*Melopsittacus undulatus*) in a wind tunnel. He observed that one specimen with a wing span b of 0.235 m flapped its wings with a constant beat frequency ω of 88 rad s^{-1} for a range of flight speeds U from 5.3 m s^{-1} to 13.3 m s^{-1}. This corresponds to a range of reduced frequencies k from 1.55 to 3.90. Similarly, Tucker (1972, 1973) measured the flapping frequency of a laughing gull (*Larus atricilla*) with a wing span b of 0.93 m to be a constant 23.8 rad s^{-1} over a range of flight speeds from 8.6 to 11.2 m s^{-1} corresponding to reduced frequencies k between 1.98 and 2.57.

In this paper, we address the problem of finding the unsteady distribution of circulation along the span of flapping wings that produces a specified lift and thrust with minimum induced losses. Induced losses include both induced drag and induced shaft power, the additional power required to flap the wings due to induced forces opposing the flapping motion. For this purpose, we adapt a theory recently developed by Hall, Yang & Hall (1994) for predicting the optimum circulation distribution for helicopters in forward flight. The method is based on the Betz (1919) criterion for minimum induced loss (M.I.L.) propellers. Goldstein (1929) used the Betz criterion to determine the optimum circulation distribution along the blades of propellers. Lighthill (1970) has alluded to the possibility of using a theory similar to Goldstein's propeller theory to predict the propulsive efficiency of swimming fish which flap their caudal fins to generate thrust. Propulsion via flapping, however, is fundamentally different from propulsion via rotation of a propeller in at least two ways. First, in the propeller problem, only thrust is developed. In the flapping problem, both thrust and lift (weight support) must be developed. Second, the optimum circulation distribution along the span of a propeller blade is constant with time. For the flapping problem, the

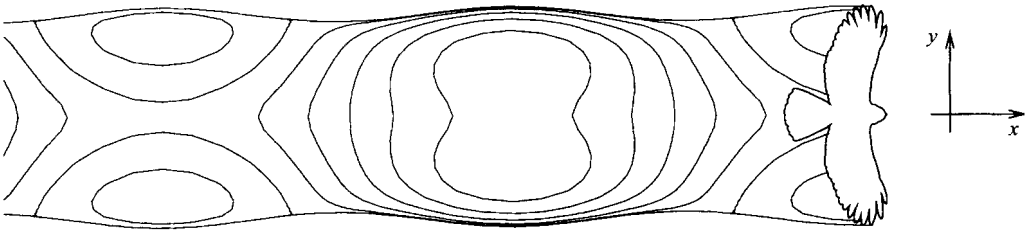

FIGURE 2. Top view of bird in flight showing coordinate system and vortex filaments (trailing and shed vorticity) in unsteady wake. (Harris' hawk planform after Tucker 1992).

spanwise circulation varies with time. Nevertheless, as we will show, the Betz criterion may be applied to flapping motion of wings (as well as helicopters in forward flight). Furthermore, because the resulting theory deals with the far wake and not the details of the flow about the wing itself, no simplifying assumptions regarding the reduced frequency or amplitude of flapping motion are required. Therefore, the present theory is applicable to high-frequency and/or large-amplitude flapping motions.

In § 2, we describe the extension of the Betz criterion for M.I.L. propellers to the case of the flapping motion of wings. In § 3, we apply the results of § 2 to the case of small-amplitude harmonic flapping motion. We show that the problem of finding the optimum spanwise circulation distribution can be reduced to a one-dimensional integral equation for the unknown circulation. This integral equation is solved efficiently using numerical quadrature. In § 4 we describe a three-dimensional vortex-lattice method for computing the optimum circulation distribution for large-amplitude period flapping motion which must simultaneously produce thrust and lift. Finally, in § 5, we conclude with a brief summary and discussion of similarities and differences between our computational results and experimental observations of bird flight.

2. Minimum induced loss flapping

2.1. *Inviscid flow model*

For the purposes of computing the induced losses due to wing flapping, we assume that the flow resulting from flapping is inviscid, incompressible, and irrotational (except for the trailing and shed vorticity in the wake). Thus, the three-dimensional flow about the wings and wake is governed by Laplace's equation,

$$\nabla^2 \phi = 0, \tag{2.1}$$

where ϕ is the usual velocity potential. The Cartesian coordinates x, y, and z are taken to be along the longitudinal, lateral, and vertical axes as shown in figure 2. Furthermore, the coordinates are fixed to the fluid frame of reference, so that the velocity of the fluid goes to zero at infinity.

In the present analysis, we assume that the flapping wing is lightly loaded. Thus, the sheet of shed and trailing vorticity (the wake) left behind the wing is only slowly convected under its own influence. For the present analysis, we therefore assume the wake is rigid, that is, the position of the wake is the trace of the position of the trailing edge of the wing. Finally, we assume that the flapping motion of the wings is periodic in time with period T. Thus, the shape of the wake is also periodic in the flight direction. Physically, of course, the wake rolls up a short distance behind the wing. Nevertheless, the assumption that the wake does not roll up and is not

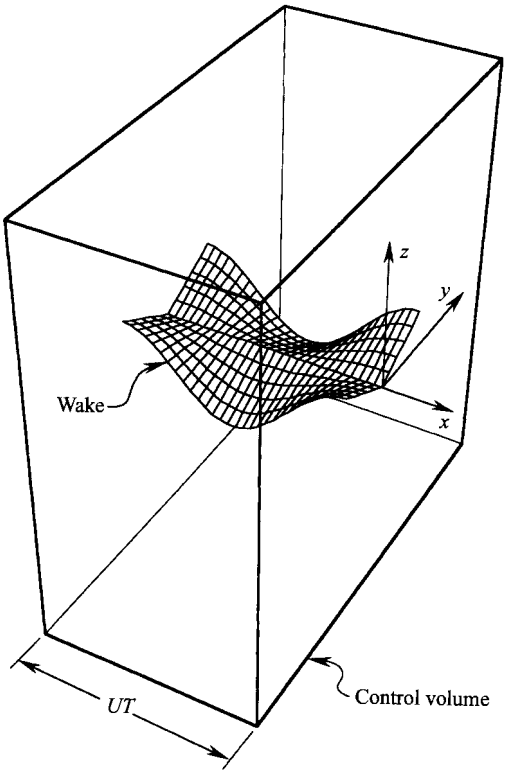

FIGURE 3. Control volume enclosing one period of the far wake.

convected greatly simplifies the subsequent analysis. Furthermore, experience in wing and propeller theory suggests that the induced losses obtained using this assumption will be in good agreement with experiment.

2.2. *Kelvin impulses*

The force (thrust, side force, and lift) acting on the flapping wing arises when the wing imparts linear momentum to the surrounding fluid. The force averaged over one period of flapping motion is equal and opposite to the time-averaged rate of change in momentum of the flow field. The linear momentum $\boldsymbol{\xi}$ deposited in the wake per temporal period T of wing flapping is given by

$$\boldsymbol{\xi} = \rho \iiint_{\mathscr{V}} \nabla\phi \, \mathrm{d}\mathscr{V}, \tag{2.2}$$

where ρ is the fluid density. In (2.2), $\mathscr{V}$ is a control volume enclosing one period of the far downstream wake and extending to infinity in the y- and z-directions (see figure 3). The integral in (2.2) is evaluated in the fluid frame of reference so that the velocity $\nabla\phi$ goes to zero as $|y|$ or $|z|$ goes to infinity.

Using Gauss' theorem, the volume integral in (2.2) may be converted to a surface integral over the surface $\mathscr{A}$ bounding the volume $\mathscr{V}$, so that

$$\boldsymbol{\xi} = -\rho \iint_{\mathscr{A}} \phi \boldsymbol{n} \, \mathrm{d}\mathscr{A}, \tag{2.3}$$

where $\boldsymbol{n}$ is the unit normal to the surface pointing into the volume $\mathscr{V}$. Since the

potential is periodic in the flight direction in the far-wake region, and since the unit normals on the fore and aft periodic boundaries of the volume point in opposite directions, the net contribution from the integration over the periodic boundaries is zero. Similarly, the potential in the far field goes to zero faster than $1/r$, where $r^2 = y^2 + z^2$, so that the contribution from the surface integral at infinity is also zero. Therefore, the only contribution to the integral in (2.3) arises from the potential on the surface of the wake itself. Hence,

$$\boldsymbol{\xi} = -\rho \iint_{\mathscr{W}} \Delta\phi \boldsymbol{n} \, \mathrm{d}\mathscr{A} = -\rho \iint_{\mathscr{W}} \Gamma \boldsymbol{n} \, \mathrm{d}\mathscr{A}, \tag{2.4}$$

where $\mathscr{W}$ is the upper surface of one period of the wake, and $\boldsymbol{n}$ is the unit normal to the wake. Also, $\Delta\phi$ is the jump in potential across the wake ($\phi_{\text{upper}} - \phi_{\text{lower}}$) and is equal to Γ, the circulation on the wing as the trailing edge of the wing passes by that point in space.

The quantity $\boldsymbol{\xi}$ is essentially the Kelvin linear impulse, and represents the increase in momentum in the fluid due to one period of wing flapping. Thus the average force per cycle acting on the flapping wings is just the negative of the Kelvin impulse $\boldsymbol{\xi}$ divided by the temporal period T of the flapping motion, so that

$$\boldsymbol{F} = -\frac{\boldsymbol{\xi}}{T} = \frac{\rho}{T} \iint_{\mathscr{W}} \Gamma \boldsymbol{n} \, \mathrm{d}\mathscr{A}. \tag{2.5}$$

Separating the force into thrust, side force, and lift components gives

$$\mathscr{T}_1 = \frac{\rho}{T} \iint_{\mathscr{W}} \Gamma \boldsymbol{i} \cdot \boldsymbol{n} \, \mathrm{d}\mathscr{A}, \tag{2.6}$$

$$\mathscr{S}_1 = \frac{\rho}{T} \iint_{\mathscr{W}} \Gamma \boldsymbol{j} \cdot \boldsymbol{n} \, \mathrm{d}\mathscr{A}, \tag{2.7}$$

$$\mathscr{L}_1 = \frac{\rho}{T} \iint_{\mathscr{W}} \Gamma \boldsymbol{k} \cdot \boldsymbol{n} \, \mathrm{d}\mathscr{A}. \tag{2.8}$$

Examination of (2.6) reveals, as expected, that thrust cannot be generated unless the unit normal to the wake $\boldsymbol{n}$ has some component in the x-direction. In other words, to generate thrust, the motion of the wings must have some motion perpendicular to the direction of flight, i.e. either up and down or side to side. Fore-and-aft motion of the wings by itself cannot generate any average thrust. Another consequence of (2.6) is that thrust can only be generated by an unsteady aerodynamic process. The subscript "1" in (2.6)–(2.8) denotes that the forces computed using Kelvin impulse technique contain only first-order effects. This is a consequence of our assumption of a rigid (lightly loaded) wake. Also note that all three components of force have the same physical origin, that is, circulation (Kutta–Joukowski 'lift').

One interesting feature of (2.5) is that the expression contains no unsteady terms. This is because our derivation is carried out in the fluid frame of reference. Recall that the wake is assumed to be convected with the unperturbed flow field. Thus, apart from higher-order roll-up effects which are ignored, the flow is steady in the fluid frame of reference, and therefore $\partial/\partial t = 0$. As an alternative, one could derive the time-averaged forces acting on the wing by enclosing the wing with a control volume fixed in the wing frame of reference, and then apply the integral form of the conservation of mass and momentum. We have included such a derivation in the Appendix. The results obtained using the control volume approach are identical to first order to those computed in this section using Kelvin impulses.

2.3. *Induced power*

The forces calculated using (2.5) do not include any induced forces, such as induced drag or induced shaft power (shaft power is the mechanical power required to flap the wings). In the present theory, we do not compute these induced forces directly. Instead, we equate the rate of work done on the fluid by the induced forces to the rate of kinetic energy deposited in the wake. The average induced power is equal to the kinetic energy deposited in the wake over one period divided by the period, so that

$$\mathscr{P}_{\text{ind}} = \frac{\rho}{2T} \iiint_{\mathscr{V}} (\nabla\phi)^2 \, \mathrm{d}\mathscr{V}. \tag{2.9}$$

Note that as defined here, the induced power $\mathscr{P}_{\text{ind}}$ is the *wasted* power. That is, the induced power is the total shaft power minus the useful thrust power,

$$\mathscr{P}_{\text{ind}} = \mathscr{P}_{\text{shaft}} - (\mathscr{T}_1 - \mathscr{D}_{\text{ind}})\, U \tag{2.10}$$

$$= \mathscr{P}_{\text{ind,shaft}} + \mathscr{P}_{\text{ind,drag}}, \tag{2.11}$$

where $\mathscr{P}_{\text{shaft}}$ is the total shaft power, $\mathscr{P}_{\text{ind,shaft}}$ is the induced shaft power equal to $\mathscr{P}_{\text{shaft}} - \mathscr{T}_1 U$, and $\mathscr{P}_{\text{ind,drag}}$ is the induced drag power equal to $\mathscr{D}_{\text{ind}} U$. Thus, induced power – which is positive by virtue of (2.9) – may be manifested as an increase in drag, an increase in shaft power, or some combination of the two.

Making use of Green's theorem, (2.9) can be rearranged to give

$$\mathscr{P}_{\text{ind}} = \frac{\rho}{2T} \left(- \iint_{\mathscr{A}} \phi \nabla\phi \cdot \boldsymbol{n} \, \mathrm{d}\mathscr{A} - \iiint_{\mathscr{V}} \phi \nabla^2 \phi \, \mathrm{d}\mathscr{V} \right). \tag{2.12}$$

The second integral term in (2.12) is identically zero since the velocity potential satisfies Laplace's equation. Furthermore, since the potential is periodic in the flight direction, and the potential goes to zero in the far field faster than $1/r$, the only contribution to the surface integral in (2.12) arises from the integration over the wake. Hence, the induced power is related to the induced wash $\boldsymbol{w}$ at the surface of the wake and the circulation Γ by

$$\mathscr{P}_{\text{ind}} = -\frac{\rho}{2T} \iint_{\mathscr{W}} \Delta\phi \nabla\phi \cdot \boldsymbol{n} \, \mathrm{d}\mathscr{A} = -\frac{\rho}{2T} \iint_{\mathscr{W}} \Gamma \boldsymbol{w} \cdot \boldsymbol{n} \, \mathrm{d}\mathscr{A}. \tag{2.13}$$

Note that the lift, thrust, and induced wash are proportional to the circulation Γ. However, the induced wash is linearly related to the vorticity, and hence the circulation in the wake, by the Biot–Savart law. Therefore, the induced power goes like the square of the circulation, and by implication is quadratic in the lift and thrust (assuming that the side force is zero). Hence, we may write

$$\mathscr{P}_{\text{ind}} = p_{11} \mathscr{L}_1{}^2 + p_{12} \mathscr{L}_1 \mathscr{T}_1 + p_{22} \mathscr{T}_1{}^2, \tag{2.14}$$

where p_{11}, p_{12}, and p_{22} are dimensional constants. In non-dimensional form, (2.14) is expressed as

$$C_{\mathscr{P}_{\text{ind}}} = k_{11} C_{\mathscr{L}_1}^2 + k_{12} C_{\mathscr{L}_1} C_{\mathscr{T}_1} + k_{22} C_{\mathscr{T}_1}^2, \tag{2.15}$$

where $C_{\mathscr{P}_{\text{ind}}}$, $C_{\mathscr{L}_1}$, and $C_{\mathscr{T}_1}$ are the coefficients of induced power, lift, and thrust respectively, and are defined by

$$C_{\mathscr{P}_{\text{ind}}} = \frac{\mathscr{P}_{\text{ind}}}{\frac{1}{2}\rho U^3 b^2}, \quad C_{\mathscr{L}_1} = \frac{\mathscr{L}_1}{\frac{1}{2}\rho U^2 b^2}, \quad C_{\mathscr{T}_1} = \frac{\mathscr{T}_1}{\frac{1}{2}\rho U^2 b^2}, \tag{2.16a,b,c}$$

and where

$$k_{11} = \tfrac{1}{2}\rho U b^2 p_{11}, \quad k_{12} = \tfrac{1}{2}\rho U b^2 p_{12}, \quad k_{22} = \tfrac{1}{2}\rho U b^2 p_{22}. \tag{2.17a,b,c}$$

Note that we have non-dimensionalized the lift, thrust, and power coefficients by the span squared rather than the wing area. We do this for two reasons. First, it simplifies the notation. Second, and more importantly, we want to emphasize the importance of span loading on the aerodynamic forces and induced power. For inviscid flows, these quantities depend only on the time history of the spanwise circulation distribution, and not the planform or aspect ratio of the wing. To convert to the conventional form of the lift coefficient, for example, one should multiply $C_{\mathscr{L}_1}$ above by the aspect ratio of the wing.

2.4. *Minimum induced loss circulation distribution*

Having described the relationship between the lift, thrust, induced power, and the circulation, we now turn to the problem of finding the optimum distribution of unsteady circulation. We seek to determine the distribution of circulation that minimizes the induced power subject to the constraint that a prescribed average lift and thrust is generated. Therefore, we define the Lagrangian power Π to be

$$\Pi = \mathscr{P}_{\text{ind}} + \boldsymbol{\lambda} \cdot (\boldsymbol{F} - \boldsymbol{F}_R), \tag{2.18}$$

where $\boldsymbol{F}_R$ is the vector of prescribed forces which in general would contain the prescribed lift $\mathscr{L}_R$, side force $\mathscr{S}_R$, and thrust $\mathscr{T}_R$. The vector $\boldsymbol{\lambda}$ is the corresponding vector of Lagrange multipliers $[\lambda_{\mathscr{T}}, \lambda_{\mathscr{S}}, \lambda_{\mathscr{L}}]^T$. To find the constrained optimum circulation distribution, one finds the circulation that makes the Lagrangian power Π stationary. Taking the variation of Π and setting the result to zero gives

$$\delta\Pi = \frac{\rho}{T} \iint_{\mathscr{W}} \left(\boldsymbol{\lambda} \cdot \boldsymbol{n} \delta\Gamma - \tfrac{1}{2} \boldsymbol{w} \cdot \boldsymbol{n} \delta\Gamma - \tfrac{1}{2} \Gamma \delta \boldsymbol{w} \cdot \boldsymbol{n} \right) \mathrm{d}\mathscr{A} + \delta\boldsymbol{\lambda} \cdot (\boldsymbol{F} - \boldsymbol{F}_R) = 0. \tag{2.19}$$

Equation (2.19) contains variations in both the circulation and the induced wash ($\delta\Gamma$ and $\delta\boldsymbol{w}$). However, the variation in the circulation and the variation in the induced wash are not independent; they are related by the reciprocity condition

$$\iint_{\mathscr{W}} \boldsymbol{w} \cdot \boldsymbol{n} \delta\Gamma \, \mathrm{d}\mathscr{A} = \iint_{\mathscr{W}} \delta \boldsymbol{w} \cdot \boldsymbol{n} \Gamma \, \mathrm{d}\mathscr{A}. \tag{2.20}$$

Equation (2.20) is a consequence of the fact that the potential ϕ is a solution of Laplace's equation. To demonstrate this, we make use of the second form of Green's theorem, i.e.

$$\iiint_{\mathscr{V}} \left(\phi_1 \nabla^2 \phi_2 - \phi_2 \nabla^2 \phi_1 \right) \mathrm{d}\mathscr{V} = - \iint_{\mathscr{A}} \left(\phi_1 \nabla \phi_2 - \phi_2 \nabla \phi_1 \right) \cdot \boldsymbol{n} \, \mathrm{d}\mathscr{A}, \tag{2.21}$$

where ϕ_1 and ϕ_2 are arbitrary functions of x, y, and z. Letting $\phi_1 = \phi$ and $\phi_2 = \delta\phi$ gives

$$\iiint_{\mathscr{V}} \left(\phi \nabla^2 \delta\phi - \delta\phi \nabla^2 \phi \right) \mathrm{d}\mathscr{V} = - \iint_{\mathscr{A}} \left(\phi \nabla \delta\phi - \delta\phi \nabla \phi \right) \cdot \boldsymbol{n} \, \mathrm{d}\mathscr{A}. \tag{2.22}$$

The left-hand side of (2.22) is zero since the potential ϕ satisfies Laplace's equation. Finally, applying arguments similar to those used to derive (2.4), (2.22) becomes

$$\iint_{\mathscr{W}} \left(\Gamma \delta \boldsymbol{w} - \delta \boldsymbol{w} \delta\Gamma \right) \cdot \boldsymbol{n} \, \mathrm{d}\mathscr{A} = 0, \tag{2.23}$$

which proves the reciprocity condition given by (2.20). Using (2.20) to eliminate $\delta\boldsymbol{w}$ in favour of $\delta\Gamma$, (2.19) becomes

$$\delta\Pi = \frac{\rho}{T} \iint_{\mathscr{W}} (\boldsymbol{\lambda} \cdot \boldsymbol{n} - \boldsymbol{w} \cdot \boldsymbol{n}) \delta\Gamma \, \mathrm{d}\mathscr{A} + \delta\boldsymbol{\lambda} \cdot (\boldsymbol{F} - \boldsymbol{F}_R) = 0. \tag{2.24}$$

The first-order necessary condition for the circulation distribution to be optimum is that $\delta\Pi = 0$ for all permissible variations in $\delta\Gamma$ and $\delta\boldsymbol{\lambda}$. Therefore, the optimality conditions are given by

$$\mathscr{T}_1 = \mathscr{T}_R, \tag{2.25}$$

$$\mathscr{S}_1 = \mathscr{S}_R, \tag{2.26}$$

$$\mathscr{L}_1 = \mathscr{L}_R, \tag{2.27}$$

and

$$\boldsymbol{w}\cdot\boldsymbol{n} = \boldsymbol{\lambda}\cdot\boldsymbol{n}. \tag{2.28}$$

The first three conditions are simply that the thrust, side force, and lift must be equal to the specified values. The fourth condition is a generalization of the Betz (1919) criterion for M.I.L. propellers. The physical interpretation is that the induced normal velocity produced by the optimum circulation distribution is identical to the normal wash one would obtain if the wake were a rigid impermeable surface translated through the fluid at velocity $\boldsymbol{\lambda}$. Thus, the optimum circulation problem is reduced to solving for the flow over an infinitely long wavy surface translating at velocity $\boldsymbol{\lambda}$; the Lagrange multiplier $\boldsymbol{\lambda}$ is selected so as to satisfy the first three necessary conditions. Note, however, that the induced wash tangent to the wake surface is not necessarily zero. Therefore the optimum circulation distribution does not necessarily produce a self-preserving wake. Furthermore, the vortex sheet may be unstable, causing the sheet to distort and roll up.

One subtlety of the present analysis merits a brief digression. Ideally, one should prescribe the total thrust, $\mathscr{T} = \mathscr{T}_1 - \mathscr{D}_{\text{ind}}$, and minimize the total shaft power, $\mathscr{P}_{\text{shaft}} = \mathscr{T}_1 U + \mathscr{P}_{\text{ind,shaft}}$. In the above analysis, we instead prescribe the first-order thrust $\mathscr{T}_1$ and minimize the sum of the induced shaft power $\mathscr{P}_{\text{ind,shaft}}$ and induced drag power $\mathscr{P}_{\text{ind,drag}} = \mathscr{D}_{\text{ind}} U$. Thus, in the end, we do not know the relative sizes of the induced shaft power and induced drag power, only the sum of the two. The choice to work with $\mathscr{T}_1$ rather that $\mathscr{T}$ is convenient, if not essential, so that the thrust will remain a first-order quantity producing a simple and elegant form for the constrained optimization problem. Fortunately, in the limit of light loading, the two approaches are asymptotically identical. To show this, consider the propulsive efficiency η_p, which is given by

$$\eta_p = \frac{\text{net thrust power}}{\text{net shaft power}} = \frac{(\mathscr{T}_1 - \mathscr{D}_{\text{ind}})\,U}{\mathscr{T}_1 U + \mathscr{P}_{\text{ind,shaft}}}. \tag{2.29}$$

The inefficiency is given by

$$1 - \eta_p = \frac{\mathscr{D}_{\text{ind}} U + \mathscr{P}_{\text{shaft}}}{\mathscr{T}_1 U + \mathscr{P}_{\text{shaft}}} \sim \frac{\mathscr{D}_{\text{ind}} U + \mathscr{P}_{\text{shaft}}}{\mathscr{T}_1 U}. \tag{2.30}$$

Thus, asymptotically, the solution of maximum propulsive efficiency is that solution which minimizes the sum of the induced drag and induced shaft powers for a prescribed first-order thrust.

3. Small-amplitude harmonic flapping

3.1. *Theory*

Consider the special case where the flapping motion of the wing is small and sinusoidal in time. The position of the wake may be expressed as

$$h(x, y) = \bar{h}(y)\sin(\alpha x), \qquad |y| \leqslant b/2, \tag{3.1}$$

where h is the z displacement of the wake. The wavenumber α in the flight direction is related to the flapping frequency by $\alpha b = k$. Thus, αb is just the reduced frequency of flapping. Without loss in generality, α is assumed here to be positive. For flapping motion which is symmetric with regard to the upstroke and downstroke as in (3.1), the optimal circulation for lift and optimal circulation for thrust problems are decoupled. Therefore, for the case where flapping must generate both thrust and lift (weight support), the optimal circulation is the sum of a steady elliptical circulation distribution, plus a sinusoidally varying circulation distribution, i.e.

$$\Gamma(x, y) = \Gamma_0(y) + \overline{\Gamma}(y; \alpha) \cos \alpha x, \tag{3.2}$$

where $\Gamma_0(y)$ is the steady (elliptical) circulation distribution required to generate the desired lift, and $\overline{\Gamma}(y;\alpha)$ is the amplitude of the circulation distribution required to generate thrust.

Considering now just the generation of thrust, we know from the previous discussion that the optimum distribution of vorticity will be such that the normal wash is identical to that one would obtain if the wake were translated in the x-direction with speed $\lambda_{\mathscr{T}}$. Hence, the optimum induced normal wash on the wake satisfies

$$w(x, y) = \lambda_{\mathscr{T}} \boldsymbol{i} \cdot \boldsymbol{n}. \tag{3.3}$$

For small-amplitude flapping ($\overline{h} \ll 1$ and $\alpha \overline{h} \ll 1$), the unit normal to the wake is given approximately by

$$\boldsymbol{n} = \boldsymbol{k} + \frac{\partial h}{\partial x}\boldsymbol{i} + \frac{\partial h}{\partial y}\boldsymbol{j}, \tag{3.4}$$

so that

$$w(x, y) = \overline{w}(y; \alpha) \cos(\alpha x) = \alpha \lambda_{\mathscr{T}} \overline{h}(y) \cos(\alpha x) \quad \text{for} \quad |y| \leqslant b/2. \tag{3.5}$$

The aerodynamic forces are found by substituting (3.2) and (3.4) into (2.6)–(2.8). The average thrust, side force, and lift are given by

$$\mathscr{T}_1 = \frac{1}{2}\rho U k \alpha \int_{-b/2}^{b/2} \overline{h}(y) \overline{\Gamma}(y; \alpha)\, \mathrm{d}y, \tag{3.6}$$

$$\mathscr{S}_1 = 0, \tag{3.7}$$

$$\mathscr{L}_1 = \rho U \int_{-b/2}^{b/2} \Gamma_0(y)\, \mathrm{d}y. \tag{3.8}$$

Next, we wish to solve for the optimum circulation distribution $\overline{\Gamma}(y;\alpha)$ that will produce the desired thrust. We begin by solving for the velocity potential ϕ. The velocity potential ϕ is governed by Laplace's equation, (2.1). Since the induced normal wash w is sinusoidal in x, the velocity potential will be sinusoidal as well, at least in the far downstream wake region. Thus, we let

$$\phi(x, y, z) = \overline{\phi}(y, z; \alpha) \cos(\alpha x). \tag{3.9}$$

Substitution of (3.9) into Laplace's equation gives

$$\frac{\partial^2 \overline{\phi}}{\partial y^2} + \frac{\partial^2 \overline{\phi}}{\partial z^2} - \alpha^2 \overline{\phi} = 0. \tag{3.10}$$

This equation is solved in the (y, z)-plane subject to the boundary conditions

$$\left.\frac{d\overline{\phi}}{dz}\right|_{z=0} = \overline{w}(y; \alpha) \quad \text{for} \quad |y| \leqslant b/2, \tag{3.11}$$

$$\bar{\phi}(y,0;\alpha) = 0 \quad \text{for} \quad |y| > b/2. \tag{3.12}$$

Note that because small-amplitude flapping motions are considered, the induced wash boundary condition may be applied at $z = 0$ rather than $z = h$. Additionally, we require that the potential go to zero at infinity, and that the potential be antisymmetric about the y-axis.

The solution to this problem is obtained using Fourier transform techniques. Fourier transforming the governing partial differential equations in the y-direction gives

$$\mathscr{F}\left(\frac{\partial^2\bar{\phi}}{\partial y^2} + \frac{\partial^2\bar{\phi}}{\partial z^2} - \alpha^2\bar{\phi}\right) = \int_{-\infty}^{+\infty}\left(\frac{\partial^2\bar{\phi}}{\partial y^2} + \frac{\partial^2\bar{\phi}}{\partial z^2} - \alpha^2\bar{\phi}\right)e^{-i\beta y}\,dy = 0, \tag{3.13}$$

so that

$$\frac{d^2\Phi^*}{dz^2} - (\alpha^2 + \beta^2)\,\Phi^* = 0, \tag{3.14}$$

where $\Phi^*(z;\alpha,\beta)$ is the Fourier transform of $\bar{\phi}(y,z;\alpha)$. The solution to (3.14) is given by

$$\Phi^*(z;\alpha,\beta) = Ae^{|z|(\alpha^2+\beta^2)^{1/2}} + Be^{-|z|(\alpha^2+\beta^2)^{1/2}}. \tag{3.15}$$

For the solution to be bounded at infinity, A must be zero. Thus, on the upper side of the symmetry plane ($z = 0^+$), we may write that

$$W^* = \frac{d\Phi^*}{dz} = -\Phi^*(\alpha^2 + \beta^2)^{12}, \tag{3.16}$$

where $W^*(\alpha,\beta)$ is the Fourier transform of the induced normal wash $\bar{w}(y;\alpha)$. Making use of the fact that the solution is antisymmetric about $z = 0$, we note that $\Gamma(x,y) = 2\phi(x,y,0^+)$, so that

$$W^* = -\tfrac{1}{2}\Gamma^*(\alpha^2 + \beta^2)^{1/2}, \tag{3.17}$$

where Γ^* is the Fourier transform of $\bar{\Gamma}$.

Next, we inverse Fourier transform (3.17) to obtain the relationship between the normal wash at the surface of the wake and the circulation. This gives

$$\bar{w}(y;\alpha) = -\frac{1}{4\pi}\int_{-\infty}^{+\infty}\Gamma^*(\alpha^2 + \beta^2)^{1/2}e^{+i\beta y}d\beta. \tag{3.18}$$

Equation (3.18) may be viewed as the inverse transform of the product of two transforms. Formally, we have that

$$\mathscr{F}^{-1}\left[(\alpha^2 + \beta^2)^{1/2}\right] = \frac{1}{\pi}\frac{\alpha^2 K_1(\alpha|y|)}{\alpha|y|}, \tag{3.19}$$

where K_1 is the first-order modified Bessel function of the second kind. The result is formal because strictly speaking the inverse transform of $(\alpha^2 + \beta^2)^n$ only exists for $n < 0$. Using the well-known result that the transform of the convolution of two functions is just the product of the transforms of the individual functions, we conclude that

$$\bar{w}(y;\alpha) = -\frac{1}{2\pi}\int_{-b/2}^{+b/2}\bar{\Gamma}(y';\alpha)\frac{\alpha^2 K_1(\alpha|y-y'|)}{\alpha|y-y'|}\,dy'. \tag{3.20}$$

Equation (3.20) is an integral equation that relates the normal wash $\bar{w}$ on the wake to the unknown circulation $\bar{\Gamma}$ and a symmetric kernel. Note that the integral in (3.20) is taken over the span of the wake since the circulation is zero outboard of the tips of the wake. The kernel in (3.20) has a second-order singularity at $y = y'$. However,

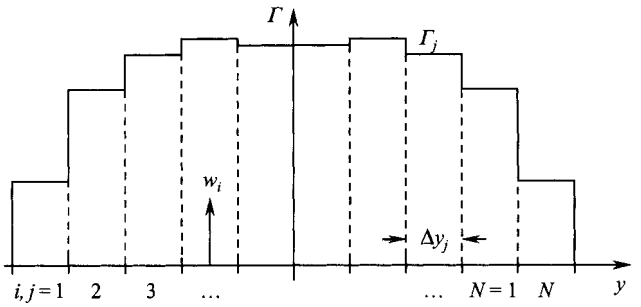

FIGURE 4. Discrete representation of circulation distribution used to compute optimum circulation distribution for small-amplitude flapping. The span of the wake is divided into a number of constant-strength circulation panels.

physically, the integral should be bounded. We conclude that the integral should be evaluated as a Mangler (1951) principal value integral.

Even though the steps taken to obtain (3.20) are strictly speaking not rigourous, the derivation is relatively straightforward and elegant. Furthermore, a more careful analysis should produce the same result. An outline of the approach is as follows. The product of transforms in (3.17) may be expressed as

$$W^* = -\frac{1}{2}(\mathrm{i}\beta\Gamma^*)\left(\frac{[\alpha^2+\beta^2]^{1/2}}{\mathrm{i}\beta}\right). \tag{3.21}$$

The inverse transform of each of the factors in parentheses in (3.21) is well defined. Because the inverse transform of the second factor has a first-order singularity, the resulting convolution integral must be interpreted as a Cauchy principal value integral. Integration by parts of the Cauchy principal value integral results in (3.20), which in turn must be interpreted as a Mangler principal value integral.

The behaviour of the kernel in (3.20) is of some interest. For small values of α (low-frequency flapping), the wake is composed predominantly of trailing vorticity and the quasi-steady kernel $1/[2\pi(y-y')^2]$ is recovered. Therefore, we may expect that for low-frequency flapping, the optimum circulation distribution will be essentially identical to the quasi-steady model of Jones (1980). For large values of α (high-frequency flapping), the wake is composed predominantly of shed vorticity and the influence of the kernel function becomes localized. Thus, in the high-frequency limit, we expect that the local circulation will be proportional to the local downwash.

3.2. *Numerical solution of the integral equation*

Except for special limiting cases, the authors know of no general closed-form solution to the above integral equation, (3.20). Therefore, in the present work, the integral equation is solved numerically. The span of the wake is divided into N panels as shown in figure 4. Over each panel, the circulation $\overline{\Gamma}$ is assumed to be a constant $\overline{\Gamma}_j$, where j denotes the jth panel. The normal wash condition, (3.20), is satisfied at N collocation points y_i at the centre of each panel so that

$$\overline{w}_i = \sum_{j=1}^{N} A_{ij}\overline{\Gamma}_j \quad \text{for} \quad i = 1, N, \tag{3.22}$$

where A_{ij} is given by

$$A_{ij} = -\frac{1}{2\pi} \oint_j \frac{\alpha^2 K_1(\alpha|y_i - y'|)}{\alpha|y_i - y'|} \, dy'. \tag{3.23}$$

In matrix form, (3.22) may be expressed as

$$\overline{w} = \boldsymbol{A}\overline{\Gamma}, \tag{3.24}$$

where $\overline{w}$ and $\overline{\Gamma}$ are vectors containing the panel values of $\overline{w}_i$ and $\overline{\Gamma}_j$.

It remains, then, to numerically evaluate the integral in (3.23), which can be done in two different ways, depending on the size of $\alpha|y_i - y_j|$. When $\alpha|y_i - y_j|$ is smaller than 3.0, the integrand is approximated using the asymptotic expression

$$\frac{K_1(|t|)}{|t|} \sim \frac{1}{t^2} + \tfrac{1}{4}(2\log|t/2| + 2\gamma - 1) + \frac{t^2}{32}(2\log|t/2| + 2\gamma - \tfrac{5}{2}) + \cdots, \tag{3.25}$$

where γ is Euler's constant ($\gamma = 0.577216...$). Substitution of this approximation into (3.23) gives

$$A_{ij} \sim \frac{\alpha}{2\pi}\left[-\frac{1}{y_i - y_{2j}} + \frac{1}{y_i - y_{1j}} + \tfrac{1}{4}(-1 + 2\gamma + 2\ln\tfrac{1}{2})\Delta y_j \right.$$

$$\left. + \tfrac{1}{2}\ln|y_i - y_{2j}|(y_i - y_{2j}) - \tfrac{1}{2}\ln|y_i - y_{1j}|(y_i - y_{1j}) + \cdots\right], \tag{3.26}$$

where y_{1j} and y_{2j} are the positions of the left and right ends of the jth panel. When $\alpha|y_i - y_j|$ is greater than 3.0 and $\Delta y_j/|y_i - y_j| \ll 1$, the integrand in (3.24) may be taken to be constant over the panel so that

$$A_{ij} \approx -\frac{1}{2\pi}\frac{\alpha^2 K_1(\alpha|y_i - y_j|)}{\alpha|y_i - y_j|}\Delta y_j. \tag{3.27}$$

For sinusoidal flapping motion, the induced power integral reduces to

$$\mathscr{P}_{\text{ind}} = -\tfrac{1}{4}\rho U \int_{-b/2}^{+b/2} \overline{\Gamma}(y;\alpha)\overline{w}(y;\alpha)\, dy. \tag{3.28}$$

Numerically, the induced power is approximated by

$$\mathscr{P}_{\text{ind}} = -\tfrac{1}{4}\rho U \sum_{i=1}^{N} \overline{\Gamma}_i \overline{w}_i \Delta y_i. \tag{3.29}$$

Substitution of (3.22) into (3.29) yields

$$\mathscr{P}_{\text{ind}} = -\tfrac{1}{4}\rho U \sum_{i=1}^{N}\sum_{j=1}^{N} A_{ij}\Delta y_i \overline{\Gamma}_i \overline{\Gamma}_j = \tfrac{1}{2}\overline{\boldsymbol{\Gamma}}^T \boldsymbol{K}\overline{\boldsymbol{\Gamma}}, \tag{3.30}$$

where the ijth entry of the matrix $\boldsymbol{K}$ is

$$K_{ij} = -\tfrac{1}{2}\rho U A_{ij}\Delta y_i.$$

Similarly, the thrust generated by flapping [see (3.6)] is approximated by

$$\mathscr{T}_1 = \tfrac{1}{2}\rho U\alpha \sum_{j=1}^{N} \overline{h}_j \overline{\Gamma}_j \Delta y_j = \boldsymbol{B}\overline{\boldsymbol{\Gamma}}, \tag{3.31}$$

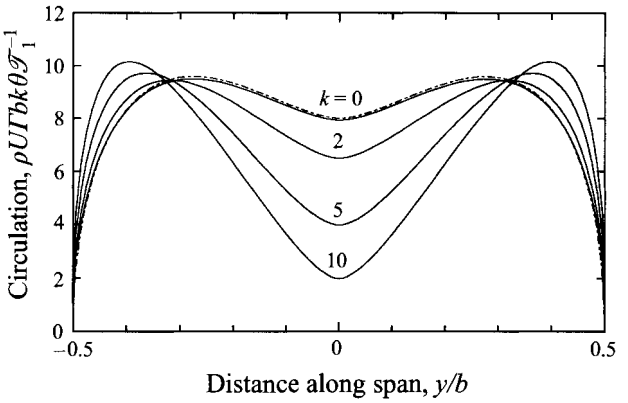

FIGURE 5. Minimum induced power circulation distributions for thrust due to flapping: ————, present small-amplitude harmonic theory; — – —, Jones (1980) quasi-steady theory.

where $\boldsymbol{B}$ is a row vector with the jth entry given by

$$B_j = \tfrac{1}{2}\rho U\alpha\bar{h}_j\Delta y_j.$$

Finally, the discrete approximation to the Lagrangian power (see (2.18)) is expressed as

$$\Pi = \tfrac{1}{2}\bar{\boldsymbol{\Gamma}}^T\boldsymbol{K}\bar{\boldsymbol{\Gamma}} + \lambda_{\mathscr{T}}\left(\boldsymbol{B}\bar{\boldsymbol{\Gamma}} - \mathscr{T}_R\right). \tag{3.32}$$

Taking the variation of (3.32) and setting it to zero gives the desired system of linear equations for the unknown circulation $\boldsymbol{\Gamma}$ and the Lagrange multiplier $\lambda_{\mathscr{T}}$,

$$\begin{bmatrix} \boldsymbol{K} & \boldsymbol{B}^T \\ \boldsymbol{B} & 0 \end{bmatrix}\begin{Bmatrix} \bar{\boldsymbol{\Gamma}} \\ \lambda_{\mathscr{T}} \end{Bmatrix} = \begin{Bmatrix} \boldsymbol{0} \\ \mathscr{T}_R \end{Bmatrix}. \tag{3.33}$$

Equation (3.33) is solved using Gaussian elimination. Typically 100 panels are used, and the assembly and solution of (3.33) requires about 0.2 s of CPU time on a Silicon Graphics Indigo R4400 workstation.

3.3. *Numerical results: M.I.L. circulation distributions for small-amplitude flapping*

In this section, we compute the circulation distributions required to generate thrust with minimum induced power for small-amplitude harmonic flapping. In all cases, we consider flapping motions given by

$$\bar{h}(y) = \theta|y| \quad \text{for} \quad |y| \leqslant b/2, \tag{3.34}$$

where θ is the amplitude of the flapping motion, with $\theta \ll 1$. Equation (3.34) describes rigid-body flapping of two halves of a wing about a common hinge point located at $y = 0$.

Using the present small-amplitude theory, the optimum circulation distribution was computed using 100 equally sized constant-strength circulation panels along the span of the wake for several different flapping frequencies k. Shown in figure 5 are the resulting circulation distributions. Also shown for comparison is the quasi-steady theory of Jones (1980). Jones was able to find an analytical solution to the minimum induced power problem for the case of quasi-steady small-amplitude flapping of the

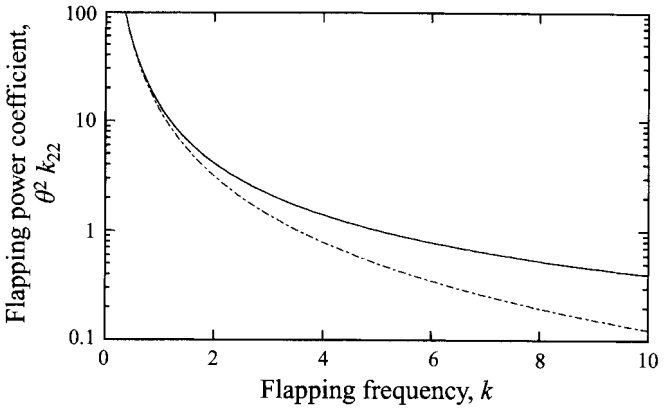

FIGURE 6. Minimum induced power requirements for thrust due to flapping: ————, present small-amplitude harmonic theory; — – —, Jones (1980) quasi-steady theory.

form given by (3.34), i.e.

$$\bar{\Gamma} = \frac{8\mathscr{T}_1}{\rho U b k \theta}\left\{\left[1 - \frac{y^2}{(b/2)^2}\right]^{1/2} + \frac{y^2}{(b/2)^2}\cosh^{-1}\left(\frac{b/2}{|y|}\right)\right\}. \tag{3.35}$$

Note the very good agreement between the present theory and the quasi-steady theory of Jones for $k = 0$. The very small differences between the exact theory of Jones and the present numerical technique are due to truncation error arising from the discretization of the integral equations ((3.22), (3.29), and (3.30)). Interestingly, the largest circulation is not at the midspan. Instead, the circulation maxima are located roughly halfway between the midspan and the tips. Furthermore, as the flapping frequency is increased, the circulation maxima move toward the tips and the circulation at the midspan diminishes. This is to be expected since for high flapping frequencies the influence of the kernel function in (3.20) becomes highly localized, and the circulation will be proportional to the local induced wash.

Shown in figure 6 is the thrust power coefficient k_{22} associated with the minimum induced power circulation distributions. Note that for small-amplitude flapping the induced power is proportional to θ^{-2}. Thus, in figure 6, we plot $\theta^2 k_{22}$ to remove the amplitude dependence. The induced power for low-frequency flapping (small k) is seen to be quite large. Also shown for comparison is the induced power predicted using the quasi-steady theory of Jones (1980). Not surprisingly, Jones' quasi-steady theory predicts lower induced power losses since the quasi-steady theory does not account for losses associated with unsteady shed vorticity in the wake.

Note that the present small-amplitude theory predicts that the minimum induced power is achieved using large-amplitude, high-frequency flapping motions. However, the small-amplitude theory is only valid when $\theta \ll 1$ and $k\theta \ll 1$. The second of these requirements is made to ensure that the normal to the wake sheet may be approximated by (3.4). The present theory may fail when either of these conditions is violated. For example, actuator disk theory predicts that the limit of the thrust power coefficient k_{22} for high-frequency flapping is $k_{22} = 1/(2\theta)$. However, the small-amplitude theory incorrectly predicts that the induced power is proportional to $1/\theta^2$ for high-frequency flapping.

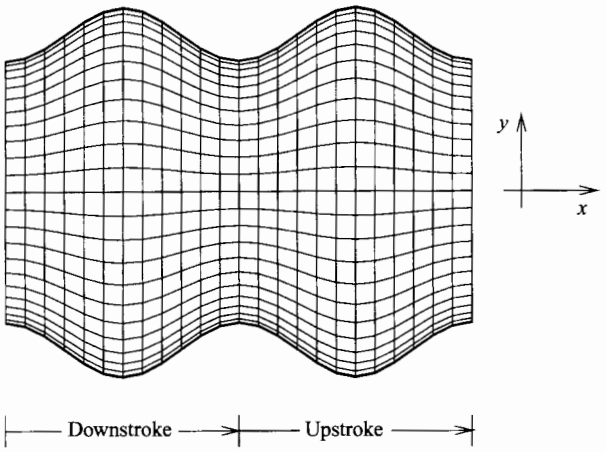

FIGURE 7. Top view of computational grid used to compute optimum circulation distributions for large-amplitude flapping. One period of the far wake is divided into a number of quadrilateral vortex ring elements.

4. Large-amplitude periodic flapping

4.1. *Vortex-lattice method*

The small-amplitude analysis of § 3 is not valid whenever the amplitude of the flapping motion, or the product of the amplitude and the frequency, is not small. To overcome these limitations, we have developed a three-dimensional vortex-lattice technique for computing the optimal distribution of circulation for large-amplitude periodic flapping.

To begin, one period of the wake is divided into a number of quadrilateral vortex ring elements as shown in figure 7. The vortex elements in the reference period of the wake are numbered 1 to N. The induced power integral, (2.13), is then approximated by

$$\mathscr{P}_{\text{ind}} = -\frac{1}{2}\frac{\rho}{T}\sum_{i=1}^{N}\Gamma_i \boldsymbol{w}_i \cdot \boldsymbol{n}_i \Delta A_i, \tag{4.1}$$

where Γ_i is the strength of the ith vortex panel, $\boldsymbol{n}_i$ is the unit normal to the ith panel, and ΔA_i is the surface area of the panel. The induced wash $\boldsymbol{w}_i$ is the wash at the centre of the ith panel, and is given by

$$\boldsymbol{w}_i = \sum_{j=1}^{N} \boldsymbol{V}_{ij}\Gamma_j, \tag{4.2}$$

where $\boldsymbol{V}_{ij}$ is the velocity at the centre of the ith panel induced by an infinite row of vortex ring panels of unit strength spaced a distance UT apart in the x-direction, with the reference sending panel located at the jth position in the grid. Standard numerical techniques are used to compute the induced wash. For panels that are close to the collocation point, the exact wash due to a quadrilateral vortex ring is computed (see for example Katz & Plotkin 1991). For panels that are far from the collocation point, the vortex ring panel is approximated by a point doublet oriented in the direction normal to the panel surface. This approximation reduces the computational time required to assemble the influence coefficients $\boldsymbol{V}_{ij}$.

Having computed the induced wash influence coefficient, we put (4.1) and (4.2) together to obtain

$$\mathscr{P}_{\text{ind}} = \tfrac{1}{2}\sum_{i=1}^{N}\sum_{j=1}^{N} K_{ij}\Gamma_i\Gamma_j = \tfrac{1}{2}\boldsymbol{\Gamma}^T\boldsymbol{K}\boldsymbol{\Gamma}, \tag{4.3}$$

where

$$K_{ij} = -\frac{\rho}{T}\boldsymbol{V}_{ij}\cdot\boldsymbol{n}_i\Delta A_i. \tag{4.4}$$

Similarly, the force $\boldsymbol{F}$ acting on the flapping wings is expressed as

$$\boldsymbol{F} = \begin{Bmatrix} \mathscr{T}_1 \\ \mathscr{S}_1 \\ \mathscr{L}_1 \end{Bmatrix} = \sum_{j=1}^{N}\boldsymbol{b}_j\Gamma_j = \boldsymbol{B}\boldsymbol{\Gamma}, \tag{4.5}$$

where $\boldsymbol{b}_j$ is the jth column of $\boldsymbol{B}$ and is given by

$$\boldsymbol{b}_j = \frac{\rho}{T}\boldsymbol{n}_j\Delta A_j. \tag{4.6}$$

Finally, the Lagrangian power is given by

$$\Pi = \tfrac{1}{2}\boldsymbol{\Gamma}^T\boldsymbol{K}\boldsymbol{\Gamma} + \boldsymbol{\lambda}\cdot(\boldsymbol{B}\boldsymbol{\Gamma} - \boldsymbol{F}_R). \tag{4.7}$$

Taking the variation of (4.7) and setting the result to zero gives the desired set of linear equations for the unknown optimal circulation distribution, i.e.

$$\begin{bmatrix} \boldsymbol{K} & \boldsymbol{B}^T \\ \boldsymbol{B} & \boldsymbol{0} \end{bmatrix}\begin{Bmatrix} \boldsymbol{\Gamma} \\ \boldsymbol{\lambda} \end{Bmatrix} = \begin{Bmatrix} \boldsymbol{0} \\ \boldsymbol{F}_R \end{Bmatrix}. \tag{4.8}$$

Equation (4.8) is solved using LU decomposition to determine the optimal distribution of circulation and the corresponding Lagrange multipliers for a prescribed thrust and lift. In this form, it is clear that the optimal circulation required to simultaneously produce both thrust and lift is equal to the sum of the optimal distribution of circulation required to generate the desired thrust but no lift and the optimal distribution of circulation required to generate the desired lift but no thrust.

4.2. *Numerical results: M.I.L. circulation distributions for propellers*

To test the accuracy of the present vortex lattice model, we first use the present vortex lattice model to compute the minimum induced power circulation distribution for a two-bladed propeller. In essence, a propeller generates thrust using 'rotational flapping' rather than reciprocal flapping about the longitudinal axis as in the case of flying animals or ornithopters. The other difference is that the lift acting on the blades of a propeller is nominally steady. Hence the wake contains only trailing vorticity, i.e. the vortex filaments form helixes. Nevertheless, the case of a propeller is useful since Goldstein (1929) has found solutions to the minimum induced loss problem for propellers with small advance ratios, a condition equivalent to large-amplitude high-frequency flapping.

Figure 8 shows the computed minimum induced loss distribution for a propeller of radius R rotating with speed Ω and generating thrust $\mathscr{T}_1$. Advance ratios μ of 0.1 and 0.5 are considered, where

$$\mu = \frac{U}{\Omega R}. \tag{4.9}$$

These solutions were computed using a vortex-lattice mesh with 32×32 vortex ring elements per turn of the wake. Also shown for comparison are the analytical results tabulated by Goldstein (1929). Since the present vortex-lattice method is a numerical

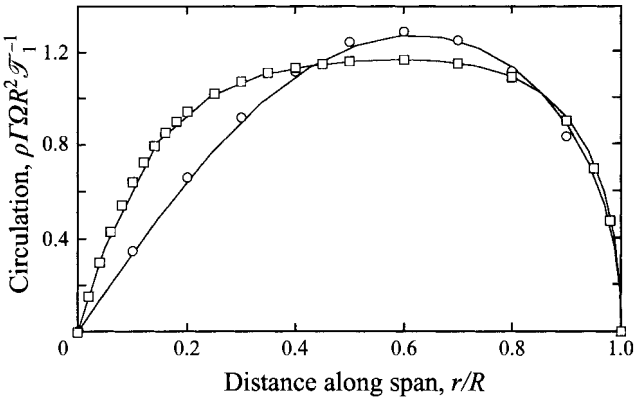

FIGURE 8. Optimum circulation distribution for two-bladed propeller at two different advance ratios: ——, present vortex-lattice method; □, Goldstein (1929) theory with advance ratio $\mu = 0.1$; ○, Goldstein (1929) theory with advance ratio $\mu = 0.5$.

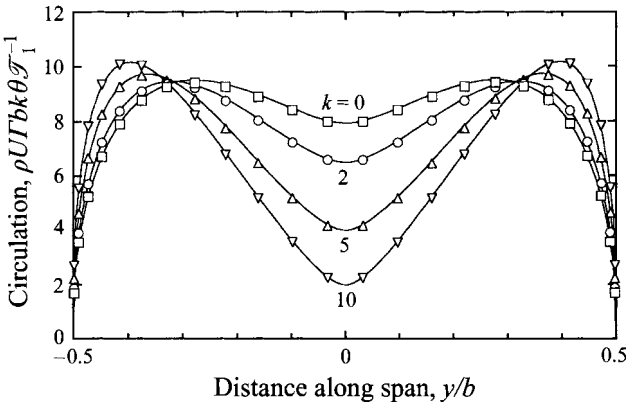

FIGURE 9. Minimum induced power circulation distributions for thrust due to flapping: ————, small-amplitude harmonic theory; □, ○, △, and ▽, vortex-lattice method with $\theta = 1°$.

approach for solving the same problem as posed by Goldstein, it is reassuring – but not surprising – that the two methods agree almost exactly. The very small differences between Goldstein's solution and the present method are due primarily to truncation error arising from the finite grid resolution (and possibly truncation error in Goldstein's original series solution).

4.3. *Numerical results: M.I.L. circulation distributions for flapping*

In this section, we compute the optimal circulation distributions and corresponding power requirements for flapping flight using the vortex-lattice method described above. We consider flapping motions where the wake has the shape

$$\left.\begin{aligned} z &= |\zeta| \sin[\theta \cos(\alpha x)] \\ y &= |\zeta| \cos[\theta \cos(\alpha x)] \end{aligned}\right\} \quad \text{for} \quad |\zeta| \leqslant b/2. \tag{4.10}$$

This motion corresponds to a wing with a straight, unswept trailing edge flapping rigidly about a hinge point on the longitudinal axis.

For the first case considered, the amplitude of flapping is small with $\theta = 1°$. Shown in figure 9 is the optimum circulation required to produce thrust. The circulation is

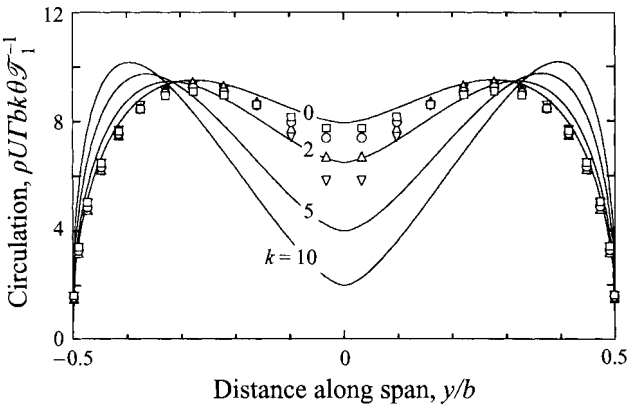

FIGURE 10. Minimum induced power circulation distributions for thrust due to flapping: ———, small-amplitude harmonic theory; □, ○, △, and ▽, vortex-lattice method with $\theta = 60°$.

plotted at the point in the downstroke when the wings pass through the horizontal position. These results were computed using a vortex-lattice mesh with 24 elements per period in the flight direction, and 24 elements in the spanwise direction. Each solution required about 69 s of CPU time to compute on a Silicon Graphics Indigo 4400 workstation. Also shown is the circulation computed using the small-amplitude harmonic theory of § 3. The two theories agree quite well for this small-amplitude case, even for flapping reduced frequencies as large as 10.

We next consider the same flapping motion described by (4.10), but with a larger amplitude, $\theta = 60°$. Figure 10 shows the optimum circulation distribution required to generate thrust. Note that the computed optimal circulation is in good agreement with the small-amplitude theory for the case where the frequency is small (the quasi-steady case). This seems to indicate that the restriction on amplitude ($\theta \ll 1$) in the small-amplitude theory will only become important when the flapping amplitude is so large that the two wing tips come close to one another. The more severe restriction on the small-amplitude theory is that $k\theta \ll 1$. The large-amplitude vortex-lattice analysis and the small-amplitude harmonic theory disagree significantly even when k is as small as 2.0 for $\theta = 60°$. When k is 5.0, there is very poor agreement between the small-amplitude theory and the vortex-lattice theory. (Presumably the latter theory is correct.)

Shown in figure 11 is the thrust power coefficient k_{22} computed using the vortex-lattice theory as a function of flapping frequency. Also shown for comparison is the induced power computed using the small-amplitude theory. For small-amplitude flapping ($\theta = 15°$), the two theories agree reasonably well, even for flapping frequencies k as large as 10. For a flapping amplitude of $\theta = 60°$, however, the minimum induced power predicted using the vortex-lattice model is considerably larger than that predicted using the small-amplitude theory, except at very low flapping frequencies. It is interesting that for the $\theta = 60°$ case, the induced power decreases rapidly with increasing flapping frequency up to a reduced frequency k of about 4 or 5. Above this frequency, the reduction in induced power is more modest, and presumably viscous profile losses would increase rapidly. By way of comparison, in low-speed flight where thrust requirements are large, the budgerigar (*Melopsittacus undulatus*) flaps its wings with a reduced frequency k of about 3.90 (Tucker 1968, 1973; private communication V. A. Tucker, 1994).

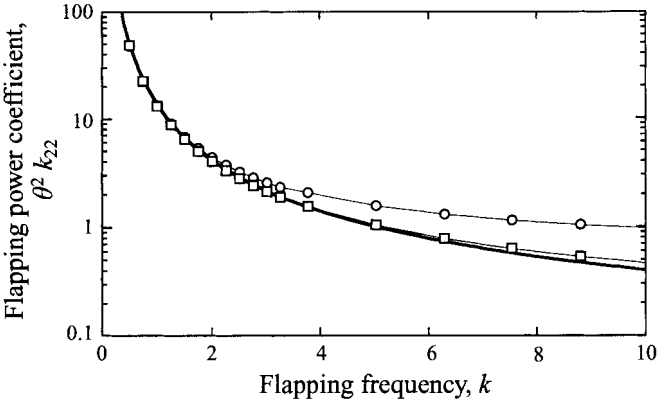

FIGURE 11. Minimum induced power requirements for thrust due to flapping: ————, small-amplitude harmonic theory; —□—, vortex-lattice method with $\theta = 15°$, —○—, vortex-lattice method with $\theta = 60°$.

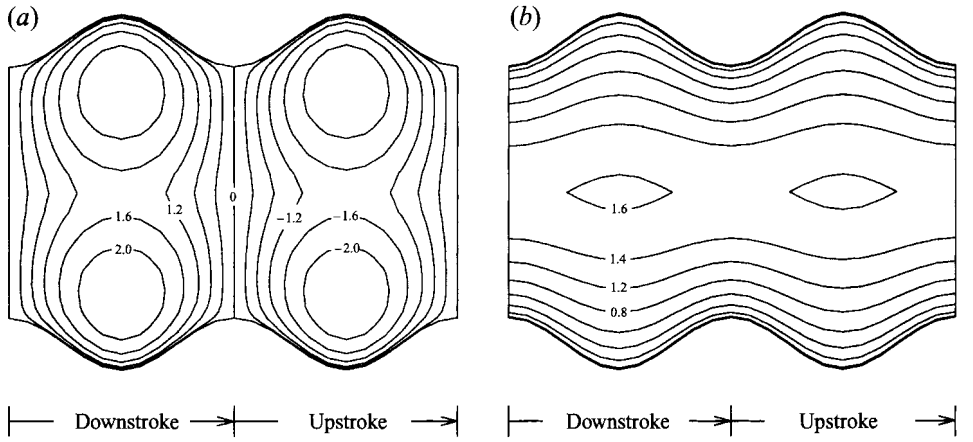

FIGURE 12. (*a*) Top view of wake showing contours of optimal circulation distribution for thrust ($\rho U \Gamma b / \mathscr{T}_1$). (*b*) Optimal circulation distribution for lift ($\rho U \Gamma b / \mathscr{L}_1$). $\theta = 45°$, $k = 5.0$.

Figure 12 shows contour plots of the circulation distribution over one period of flapping motion for the case where the amplitude of flapping motion θ is 45°, and the reduced frequency k is π. The distribution of circulation for lift is nearly constant at each spanwise station (the wavy contours are primarily a result of the apparent shortening of the wing span in the (x,y)-plane due to large-amplitude flapping). In contrast, the distribution of circulation for thrust produces primarily shed vorticity, especially at the top and bottom of the stroke. Also, we note that for this large-amplitude high-frequency case the circulation distribution is periodic in time, but not sinusoidal. In fact, in the limit of very large frequency, all of the shed vorticity occurs at the top and bottom of the stroke, and all of the trailing vorticity occurs at the tips. The result is an 'actuator disk' model in which all of the vorticity occurs along the trace of the outline of the disk, in this case the area in the (y,z)-plane swept out by the wings.

For the case where both lift and thrust must be generated, the optimum circulation distribution will be a linear combination of those shown in figure 12. Figure 13

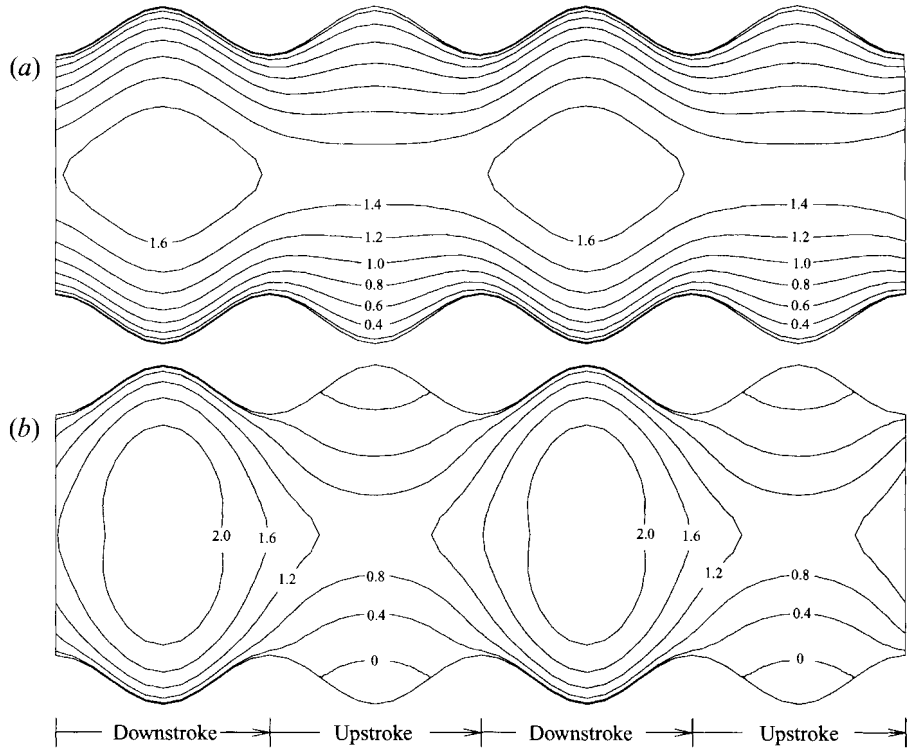

FIGURE 13. Top view of wake showing contours of optimal circulation distribution for flapping motion that must simultaneously produce lift and thrust. $k = 5.0$, $\theta = 45°$. (*a*) $\mathscr{T}_1/\mathscr{L}_1 = 0.1$, (*b*) $\mathscr{T}_1/\mathscr{L}_1 = 0.4$. For both cases, contours of $\rho U\Gamma b/\mathscr{L}_1$ are shown.

shows the optimal circulation distribution in the wake for two cases: $\mathscr{T}_1/\mathscr{L}_1 = 0.1$ and $\mathscr{T}_1/\mathscr{L}_1 = 0.4$. The first is representative of fast forward flight (cruise) where the thrust requirements are modest. The second case corresponds to slow flight or climbing flight where the thrust requirements are more severe. Note in the case of $\mathscr{T}_1/\mathscr{L}_1 = 0.1$, few of the vortex filaments form closed loops. Thus, we may expect that this wake will roll up into two undulating finite-core vortices. Because on the upstroke the vortex filaments are on average more inboard than on the downstroke (see figure 13), the rolled-up vortices will tend to be more inboard on the upstroke. This situation is qualitatively similar to the 'concertina wake' described by Pennycuick (1988) and the 'continuous-wake gait' described by Rayner (1991, 1993), and observed by Spedding (1986) and others for birds in fast forward flight.

In contrast, for the case where $\mathscr{T}_1/\mathscr{L}_1 = 0.4$, the filaments of vorticity for the optimal circulation distribution form a sheet of concentric vortex rings on the downstroke, with a sheet of predominately trailing vorticity during the upstroke. When rolled up, we would expect the wake to consist of finite-core vortex rings connected by a pair of finite-core trailing vortices. This situation is qualitatively similar to the ladder wake described by Pennycuick (1988). Also note that during the upstroke the circulation is quite small near the tips. Thus, since the wing is relatively inactive near the tips, it may be advantageous to reduce the span of the wing on the upstroke to reduce viscous drag.

Figure 14 shows the minimum induced power coefficient for thrust, k_{22}, as a function of flapping amplitude for several different flapping frequencies. Also shown

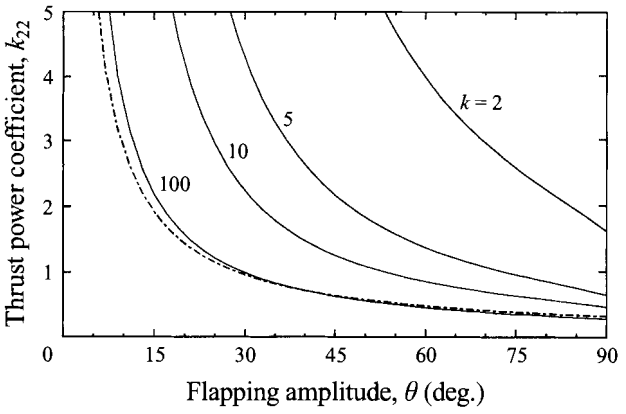

FIGURE 14. Minimum induced power required to generate thrust using large-amplitude flapping for several different flapping frequencies: ————, vortex-lattice method; — – —, actuator disk theory.

for comparison is the induced power predicted using lightly loaded actuator disk theory where the actuator disk area A is taken to be the area in the (y, z)-plane swept out by the flapping motion, $A = \theta b^2$. Actuator disk theory should provide the theoretical lower limit to the minimum induced power requirements for high flapping frequencies.† Note that the induced power required for thrust decreases with increasing flapping amplitude and flapping frequency. Also, as expected, the induced power due to flapping is generally higher than predicted using actuator disk theory. However, as the flapping frequency and amplitude get large, the induced power approaches the actuator disk limit (the present theory slightly under-predicts the induced power due to numerical truncation error).

Another interesting feature of large-amplitude flapping is the trade-off between the induced power associated with thrust and lift. To generate a certain lift and thrust at a given flapping frequency, there exists an optimum flapping amplitude. To understand this phenomenon, consider the induced power required to generate lift, k_{11}. Shown in figure 15 is the induced power required to generate lift as a function of flapping amplitude for several different flapping frequencies. Note that for small-amplitude flapping, the induced power coefficient approaches $1/\pi$ (to within truncation error) corresponding to the optimal elliptical distribution of circulation for a planar wing. For larger amplitudes, the effective span of the wing is reduced on average, and hence the average circulation must increase resulting in larger induced power losses. The trend of increasing induced power with flapping amplitude is opposite to the trend in the case of thrust. Thus, there will exist an optimum flapping amplitude that minimizes the induced power required to simultaneously generate lift and thrust.

One subtlety with the present analysis is that it predicts the induced power, but not the form of the induced power (see §2.3, (2.9)–(2.11)). For example, in gliding flight, the induced power manifests itself as induced drag opposing the forward motion of the wing. In flapping flight, however, the induced power may appear as induced drag, or

† Theodorsen (1948, p. 31) has asserted that for propellers, actuator disk theory is not the limit of minimum induced loss theory as the rotational frequency of the propeller goes to infinity. In fact, the limiting induced power of a M.I.L. propeller is slightly larger than predicted by actuator disk theory, but typically no more than about 1% more (Ribner & Foster 1990). We may expect a similar result for flapping.

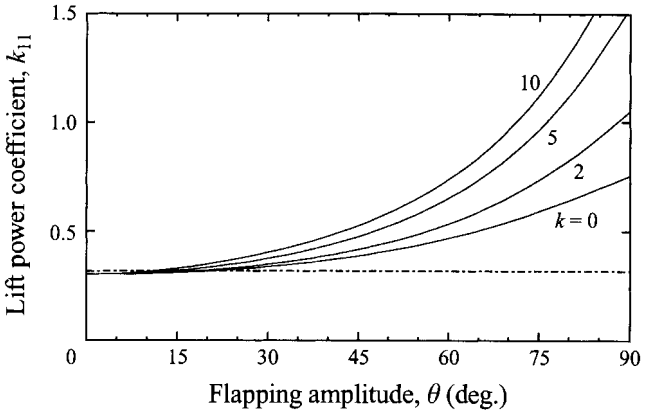

FIGURE 15. Minimum induced power required to generate lift using large-amplitude flapping for several different flapping frequencies: ———, vortex-lattice method; — — —, planar wing limit, $k_{11} = 1/\pi$.

as induced shaft power, or as a combination of the two. If the induced power appears entirely as induced shaft power, then additional shaft power must be expended to flap the wings. If, on the other hand, the induced power appears as induced drag, then additional power must be expended to produce the additional thrust to overcome the induced drag. But since the production of thrust is inefficient, some additional induced drag will result. The latter case is clearly less desirable. However, for small-amplitude motions, the induced power appears entirely as induced drag. Thus, for the present analysis, we assume that the same is true for large-amplitude motions. While an approximation, this assumption is thought to provide an upper bound on the minimum induced power required for sustained flight, and a reasonable estimate of the induced power for moderate flapping amplitudes. Furthermore, one can easily show that for light loading, the form of the induced power has only a higher-order influence on the propulsive efficiency.

Consider the case where a flapping wing must generate lift, provide sufficient thrust to overcome profile and parasitic drag, provide thrust to climb, and provide thrust to overcome any induced drag. The resulting force balance in the flight direction can be expressed as

$$\mathscr{T}_1 U = p_{11}\mathscr{L}_1^2 + p_{12}\mathscr{L}_1\mathscr{T}_1 + p_{22}\mathscr{T}_1^2 + \mathscr{D}_{\text{ext}}U, \tag{4.11}$$

where we have lumped the profile drag, parasitic drag, and the component of force due to gravity opposite to the direction of flight into a single 'external' drag term $\mathscr{D}_{\text{ext}}$. Solving for the thrust required to maintain unaccelerated flight and non-dimensionalizing the result, we find that the coefficient of thrust is given by

$$C_{\mathscr{T}_1} = \frac{1 - k_{12}C_{\mathscr{L}_1} - \left[(1 - k_{12}C_{\mathscr{L}_1})^2 - 4k_{22}(k_{11}C_{\mathscr{L}_1}^2 + C_{\mathscr{D}})\right]^{1/2}}{2k_{22}}. \tag{4.12}$$

Under the assumption that all the induced power appears as induced drag, the coefficient of thrust will also be equal to the coefficient of total shaft power. As an example, consider the case where the coefficient of lift $C_{\mathscr{L}_1}$ is equal to 0.1. Shown in figure 16 is the coefficient of thrust for several coefficients of external drag as a function of flapping amplitude for a flapping frequency k equal to π. Note that in each case there is an optimum flapping amplitude which gives a minimum coefficient of thrust (and hence flapping power). As the external drag increases, the optimum

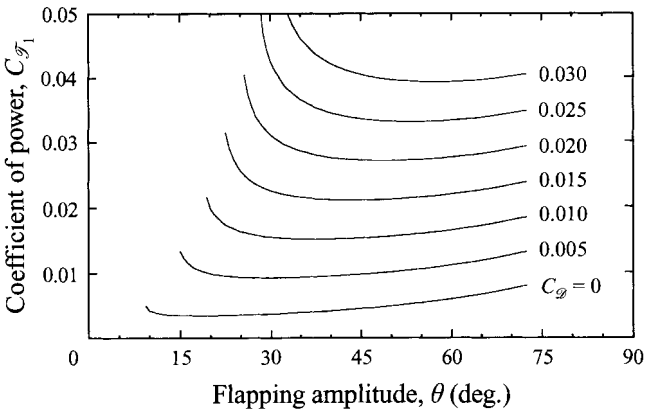

FIGURE 16. Total power required to maintain unaccelerated flight. $C_{\mathscr{L}_1} = 0.1$, $k = \pi$.

flapping amplitude increases. This is to be expected since generally more thrust will be required, and the power required for thrust decreases with increasing flapping amplitude.

Finally, we quantify the induced propulsive efficiency for flapping. The propulsive efficiency η is defined here as the total drag in gliding flight times the flight velocity divided by the power provided required to flap the wings. Hence,

$$\eta = \frac{k_{11}^0 C_{\mathscr{L}_1}^2 + C_{\mathscr{D}}}{C_{\mathscr{T}_1}}, \tag{4.13}$$

where k_{11}^0 is the lift power coefficient for non-flapping flight, and is equal to $1/\pi$. Using this definition, one finds that for a coefficient of lift $C_{\mathscr{L}_1}$ equal to 0.1, and a coefficient of external drag $C_{\mathscr{D}}$ equal to 0.01, the maximum propulsive efficiency is 88.2% corresponding to an optimum flapping amplitude of 37°. For $C_{\mathscr{D}}$ equal to 0.03, the maximum propulsive efficiency is 85.5% corresponding to an optimum flapping amplitude of about 58°. Thus, flapping is seen to be a remarkably efficient form of propulsion.

5. Summary and discussion

The Betz criterion has been applied to the problem of flapping as a means of simultaneously generating thrust and lift in forward flight. The physical interpretation of the Betz criterion is that the optimal induced normal wash on the wake is equivalent to the normal wash on an impermeable surface which has the shape of the vortex trace, and which is translated with velocity λ through an inviscid, irrotational fluid at rest at infinity. The optimal circulation on the wake, which in turn gives the time history of the optimal circulation along the span of the flapping wings, is equal to the potential jump across the impermeable surface.

For small-amplitude harmonic motion, a one-dimensional integral equation for the unknown circulation distribution was derived. The integral equation can be solved quite efficiently using numerical quadrature. For low-frequency flapping, the present theory correctly reproduces the results of the quasi-steady theory of Jones (1980). Notwithstanding the assumption of small-amplitude flapping motion, the method predicts that the highest propulsive efficiencies will be produced when the amplitude and frequency of the flapping motion is large.

For more general large-amplitude flapping motions, a vortex-lattice method was developed for computing the optimal circulation distribution. This method was compared to three other theories. For low-frequency small-amplitude motions, the present vortex-lattice theory recovers the circulation distribution predicted by Jones (1980). To test the results for large-amplitude, high-frequency flapping motions, we compared the results of the present theory to Goldstein's (1929) propeller theory and found them to be in excellent agreement. Finally, in the limit of very high flapping frequency, the predicted induced power for flapping to produce thrust approaches the theoretical limit of actuator disk theory.

Using the vortex-lattice theory, we computed the optimal circulation distribution required to simultaneously generate thrust and lift for a prescribed wing beat. For low values of thrust to lift, the optimal solutions consists primarily of trailing vorticity. For this case, the physical wake will roll up into two undulating vortices similar to the concertina wake described by Pennycuick (1988) or the continuous-vortex wake described by Rayner (1991, 1993). For the large thrust-to-lift case, the vortex filaments for the optimal distribution form a sheet of concentric vortex rings on the downstroke. These vortex rings are 'connected' by a sheet of predominately trailing filaments on the upstroke. In other words, the wing is aerodynamically active on both the upstroke and downstroke, much like the ladder-wake gait described by Pennycuick (1988). This result is in contrast to the experimental observation of wakes behind slow flying birds and bats, e.g. Spedding *et al.* (1984) and Spedding (1986). In the experiments described in these studies, the wake appears to be composed of a chain of distinct finite-core vortices. In fact, Rayner (1991) goes so far as to claim that the ladder-wake gait is never used by vertebrates.

There are a number of possible explanations for the differences between the present theory and the experimental observations. First, the present theory predicts the optimal aerodynamic solution. Animals may generate lift and thrust suboptimally (from an aerodynamic point of view), or the optimal solution adapted by animals may take into account important effects not included in the present study. For example, the physiological efficiency of the muscles in the conversion of energy into shaft power is not modelled here, nor are viscous effects. Second, we note that in some of the experimental data, the wing may in fact be aerodynamically active on the upstroke, but the relatively weak trailing vorticity may not be visible in the rolled-up wake. In fact, there is some experimental evidence supporting this conjecture. In two experimental studies, Spedding *et al.* (1984) and Spedding (1986) found that the momentum contained in the wake consisting of finite-core vortex rings of the size and strength measured in the experiments provided only 35% to 50% of the lift required to support the weight of slow-flying birds. Quoting Spedding (1986), "From the numerical results, it seems that a simple vortex ring model fails as an accurate experimental description of the wake... If a chain of vortex rings is the most appropriate qualitative description of the wake, it is still a simplified one which, from an experimental point of view, results in a significant amount of the wake momentum being ignored." Some of this missing momentum may be contained in trailing vorticity in the upstroke portion of the wake, as suggested by the results presented in figure 13. Third and finally, the present description of the kinematics of the wing motion may be too simplistic. For instance, most birds flex their wings at the wrist on the upstroke. In the present study, however, the wing was assumed rigid. The flexing of bird wings may produce useful aerodynamic benefits not reflected in the examples presented in this paper. Nevertheless, the methods described here may be used to analyse the aerodynamics of flexible flapping motions.

The present analysis is a first-order theory, i.e. it does not address wake roll-up. We would argue, however, that wake roll-up does not significantly affect the optimal circulation distribution. This is not to say that the wake does not roll up – it does. Instead we would assert that for light loading the roll-up has little influence on the flow near the wing. For instance, propellers may be regarded as generating thrust by large-amplitude 'rotational flapping.' The wake left behind the propeller is helical in shape, and successive turns of the wake may be quite close to one another. The wake rapidly rolls up forming a chaotic circular jet behind the propeller. Nevertheless, the classical first-order propeller theory of Goldstein (1929) works quite well, and is still used to design propellers of high efficiency.

We emphasize that the models presented in this paper address only the induced losses associated with wing flapping. A more complete theory would also account for profile and parasitic losses. As in propellers, profile losses will be large for large reduced frequencies since the relative velocity will be large and the viscous power goes roughly like the cube of the relative velocity. At very low reduced frequencies, on the other hand, the sectional lift required to generate a given thrust gets large since the unit normal to the wake is nearly perpendicular to the direction of flight. Large coefficients of sectional lift generally imply large coefficients of sectional viscous drag. Therefore, one would expect that in addition to an optimum flapping amplitude, there would also exist an intermediate optimum flapping frequency. In fact, the viscous forces may alter the optimum circulation distribution rendering the inviscid load distributions suboptimal. One simple but approximate approach for high-aspect-ratio wings is to assume that the reduced frequency based on wing span is $O(1)$, but the reduced frequency based on aerodynamic chord is small. Thus, inviscid power losses can be modelled as described in this paper, with viscous profile losses modelled at each spanwise station using quasi-steady drag polar correlations of airfoil sections. The first author is currently exploring this approach with applications to carangiform swimming, and will report the results in a forthcoming paper (Hall 1996).

The authors would like to thank Professor Vance A. Tucker of the Department of Zoology at Duke University for his useful comments on various aspects of bird flight, and for providing the digitized data of the planform of the Harris' hawk used in figure 2.

Appendix. Alternative derivation of thrust and power

In § 2, the lift, side force, thrust, and power associated with flapping were computed using impulse and energy considerations. An explicit assumption in that derivation was that the wings were lightly loaded. In this Appendix, these quantities are rederived using integral conservation statements for both the general loading (§ A.1 and § A.2) and light loading cases (§ A.3). We consider the situation where the flapping motion may be large and periodic in time.

A.1. *Thrust, side force, and lift*

Consider first the calculation of the time-averaged aerodynamic forces (the thrust, side force, and lift). For convenience, the calculations are performed in an inertial reference frame translating with the wing. In this frame of reference, the far-field flow is in the positive x-direction with speed U. Now suppose the wing is enclosed in a control volume (CV) fixed in space bounded by a control surface (CS) as shown schematically in figure 17. The aft portion of the control surface is the 'Trefftz plane',

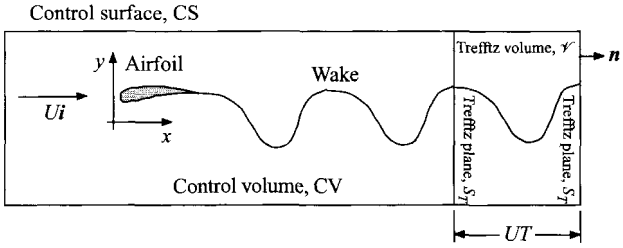

FIGURE 17. Two-dimensional sketch of conventional control volume and 'Trefftz volume' used to compute time-averaged aerodynamic forces and power.

and is taken to be normal to the direction of flight. Application of the integral form of the conservation of momentum gives

$$-\boldsymbol{F}(t) - \iint_{\mathrm{CS}} p\boldsymbol{n}\,\mathrm{d}\mathscr{A} = \frac{\mathrm{d}}{\mathrm{d}t}\iiint_{\mathrm{CV}} \rho \boldsymbol{V}\,\mathrm{d}\mathscr{V} + \iint_{\mathrm{CS}} \rho \boldsymbol{V}\boldsymbol{V}\cdot\boldsymbol{n}\,\mathrm{d}\mathscr{A}, \tag{A 1}$$

where here $\boldsymbol{F}(t)$ represents the instantaneous force acting on the wing ($-\boldsymbol{F}(t)$ is the force exerted by the wing on the fluid), $\boldsymbol{n}$ is the outward unit normal to the control surface, and $\boldsymbol{V}$ is the fluid velocity given by

$$\boldsymbol{V} = U\boldsymbol{i} + \nabla\phi = (U+u)\boldsymbol{i} + v\boldsymbol{j} + w\boldsymbol{k}. \tag{A 2}$$

In this frame of reference, the flow is unsteady. The static pressure p is given by the unsteady form of Bernoulli's equation, i.e.

$$p = p_\infty + \tfrac{1}{2}\rho U^2 - \tfrac{1}{2}\rho \boldsymbol{V}^2 - \rho\frac{\partial\phi}{\partial t} = p_\infty - \tfrac{1}{2}\rho\left(2Uu + u^2 + v^2 + w^2 + 2\frac{\partial\phi}{\partial t}\right). \tag{A 3}$$

Substitution of (A 2) and (A 3) into (A 1) gives, after some manipulation,

$$\boldsymbol{F}(t) = -\frac{\mathrm{d}}{\mathrm{d}t}\iiint_{\mathrm{CV}} \rho\boldsymbol{V}\,\mathrm{d}\mathscr{V} + \iint_{\mathrm{CS}} \tfrac{1}{2}\rho\left(2Uu + u^2 + v^2 + w^2 + 2\frac{\partial\phi}{\partial t}\right)\boldsymbol{n}\,\mathrm{d}\mathscr{A}$$
$$- \iint_{\mathrm{CS}} \rho U\boldsymbol{i}\boldsymbol{V}\cdot\mathrm{d}\mathscr{A} - \iint_{\mathrm{CS}} \rho(u\boldsymbol{i} + v\boldsymbol{j} + w\boldsymbol{k})\boldsymbol{V}\cdot\boldsymbol{n}\,\mathrm{d}\mathscr{A}. \tag{A 4}$$

Application of conservation of mass reveals that the third integral in (A 4) is identically zero. Also, except on the Trefftz plane, the perturbation velocities and velocity potentials decay faster than r^{-2}, where r is the distance from the wake, so that the surface integrals go to zero if the control volume is placed far from the wing, except on the Trefftz plane which intersects the wake. Therefore, after some rearranging, the instantaneous force on the wing may be expressed as

$$\boldsymbol{F}(t) = -\frac{\mathrm{d}}{\mathrm{d}t}\iiint_{\mathrm{CV}} \rho\boldsymbol{V}\,\mathrm{d}\mathscr{V} + \iint_{S_T} \tfrac{1}{2}\rho\left(2\frac{\partial\phi}{\partial t} - u^2 + v^2 + w^2\right)\boldsymbol{i}\,\mathrm{d}y\,\mathrm{d}z$$
$$- \iint_{S_T} \rho(v\boldsymbol{j} + w\boldsymbol{k})(U+u)\,\mathrm{d}y\,\mathrm{d}z, \tag{A 5}$$

where S_T denotes the Trefftz plane.

The presence of the time-dependent volume integral makes it impossible to calculate the instantaneous force acting on the wing without knowing the details of the flow everywhere in the control volume. However, we are interested here in the time-averaged forces. Therefore, (A 5) is multiplied by $\mathrm{d}t$, integrated over one time period,

and the result divided by the period T to obtain the average forces, i.e.

$$\boldsymbol{F} = \frac{1}{T}\int_t^{t+T}\iint_{S_T} \tfrac{1}{2}\rho\left(2\frac{\partial\phi}{\partial t} - u^2 + v^2 + w^2\right)\boldsymbol{i}\,\mathrm{d}y\,\mathrm{d}z\,\mathrm{d}t$$

$$- \frac{1}{T}\int_t^{t+T}\iint_{S_T} \rho(v\boldsymbol{j} + w\boldsymbol{k})(U+u)\,\mathrm{d}y\,\mathrm{d}z\,\mathrm{d}t. \tag{A 6}$$

Note that the first term in (A 5) does not appear in (A 6). This is because when multiplied by dt, that term is an exact differential. Since the flow is temporally periodic, the result of the integration over one period is zero.

Taking the scalar product of (A 6) with $-\boldsymbol{i}$, $\boldsymbol{j}$, and $\boldsymbol{k}$ gives the time-averaged thrust, side force, and lift, respectively. These are

$$\mathscr{T} = \frac{1}{T}\int_t^{t+T}\iint_{S_T} \tfrac{1}{2}\rho\left(2\frac{\partial\phi}{\partial t} - u^2 + v^2 + w^2\right)\mathrm{d}y\,\mathrm{d}z\,\mathrm{d}t, \tag{A 7}$$

$$\mathscr{S} = -\frac{1}{T}\int_t^{t+T}\iint_{S_T} \rho v(U+u)\,\mathrm{d}y\,\mathrm{d}z\,\mathrm{d}t, \tag{A 8}$$

$$\mathscr{L} = -\frac{1}{T}\int_t^{t+T}\iint_{S_T} \rho w(U+u)\,\mathrm{d}y\,\mathrm{d}z\,\mathrm{d}t. \tag{A 9}$$

In the integral in (A 7), one might be tempted to interpret the term $(\partial\phi/\partial t)\,\mathrm{d}t$ as an exact differential, and thus conclude that that portion of the integral is zero since the unsteady flow is period in time. However, the potential is only periodic so long as one does not pass through the wake. On the Trefftz plane, the wake oscillates periodically so that in some regions of the Trefftz plane, the wake is crossed as time advances. Thus the unsteady potential is not temporally periodic. The physical interpretation is that (first-order) thrust can only be generated if the wake undergoes unsteady motion normal to the direction of flight.

Finally, we emphasize that (A 7)–(A 9) are exact even for heavily loaded wings provided that the flow is incompressible, inviscid, and irrotational except for trailing and shed vorticity in the wake.

A.2. *Flapping power*

Next, we compute the mechanical power required to flap the wings. The integral form of the conservation of energy is

$$-\mathscr{P}_{\mathrm{shaft}}(t) - \iint_{\mathrm{CS}} p\boldsymbol{V}\cdot\boldsymbol{n}\,\mathrm{d}\mathscr{A} = \frac{\mathrm{d}}{\mathrm{d}t}\iiint_{\mathrm{CV}} \tfrac{1}{2}\rho\boldsymbol{V}^2\,\mathrm{d}\mathscr{V} + \iint_{\mathrm{CS}} \tfrac{1}{2}\rho\boldsymbol{V}^2\boldsymbol{V}\cdot\boldsymbol{n}\,\mathrm{d}\mathscr{A}, \tag{A 10}$$

where $\mathscr{P}_{\mathrm{shaft}}(t)$ is the instantaneous mechanical power required to flap the wings ($-\mathscr{P}_{\mathrm{shaft}}(t)$ is the rate at which the wings do work on the fluid). Again, making use of Bernoulli's equation and noting that the perturbation quantities fall to zero faster than r^{-2} gives

$$\mathscr{P}_{\mathrm{shaft}}(t) = -\frac{\mathrm{d}}{\mathrm{d}t}\iiint_{\mathrm{CV}} \tfrac{1}{2}\rho\boldsymbol{V}^2\,\mathrm{d}\mathscr{V} - \iint_{S_T} \rho\frac{\partial\phi}{\partial t}(U+u)\,\mathrm{d}y\,\mathrm{d}z. \tag{A 11}$$

Finally, averaging the power over one period gives

$$\mathscr{P}_{\mathrm{shaft}} = +\frac{1}{T}\int_t^{t+T}\iint_{S_T} \rho\frac{\partial\phi}{\partial t}(U+u)\,\mathrm{d}y\,\mathrm{d}z\,\mathrm{d}t, \tag{A 12}$$

where the first term in (A 11) integrates to zero because when multiplied by dt it is an exact differential.

Finally, the average *induced power* $\mathscr{P}_{\text{ind}}$ is defined as the difference between the average power and the thrust power, and is given by

$$\begin{aligned}\mathscr{P}_{\text{ind}} &= \mathscr{P}_{\text{shaft}} - U\mathscr{T} \\ &= \frac{1}{T}\int_t^{t+T}\iint_{S_T} \tfrac{1}{2}\rho U(-u^2+v^2+w^2)\,\mathrm{d}y\,\mathrm{d}z\,\mathrm{d}t \\ &\quad + \frac{1}{T}\int_t^{t+T}\iint_{S_T} \rho U\frac{\partial\phi}{\partial t}u\,\mathrm{d}y\,\mathrm{d}z\,\mathrm{d}t. \end{aligned} \tag{A 13}$$

Again, (A 13) is exact provided the flow is inviscid, incompressible, and irrotational.

A.3. *Light loading approximations*

For most cases of practical interest (except hover and slow forward flight), the assumption of light loading is valid, that is, $|\nabla\phi| \ll U$. Under these circumstances, the unsteady wake and associated potential are simply convected in the x-direction with speed U. Thus, $\phi = \phi(x - Ut, y, z)$ to leading order so that

$$\frac{\partial\phi}{\partial t} = -Uu. \tag{A 14}$$

Also, since in the light-loading approximation the unsteady flow is simply convected in the x-direction, averaging over one temporal period is equivalent to averaging over one spatial period. Therefore, to first order, (A 6) becomes

$$\boldsymbol{F} = -\frac{1}{T}\iiint_{\mathscr{V}} \rho(u\boldsymbol{i} + v\boldsymbol{j} + w\boldsymbol{k})\mathrm{d}\mathscr{V}, \tag{A 15}$$

where $\mathscr{V}$ is the 'Trefftz volume', the volume contained between two Trefftz planes a distance UT apart.

Similarly, using the light-loading assumption, the average induced power (A 13) is to leading order given by

$$\mathscr{P}_{\text{ind}} = \frac{1}{T}\iiint_{\mathscr{V}} \tfrac{1}{2}\rho(u^2+v^2+w^2)\mathrm{d}\mathscr{V}. \tag{A 16}$$

In words, the induced power for lightly loaded systems is just the rate at which kinetic energy as measured in the fluid frame of reference is deposited into the wake. Equation (A 16) is valid for both planar and non-planar wakes.

REFERENCES

AHMADI, A. R. & WIDNALL, S. E. 1985 Unsteady lifting-line theory as a singular-perturbation problem. *J. Fluid Mech.* **153**, 59–81.

AHMADI, A. R. & WIDNALL, S. E. 1986 Energetics and optimum motion of oscillating lifting surfaces of finite span. *J. Fluid Mech.* **162**, 261–282.

BETTERIDGE, D. S. & ARCHER, R. D. 1974 A study of the mechanics of flapping wings. *Aero. Q.* **25**, 129–142.

BETZ, A. 1919 Schraubenpropeller mit geringstem Energieverlust. *Göttinger Nachrichten*, p. 193.

GOLDSTEIN, S. 1929 On the vortex theory of screw propellers. *Proc. R. Soc. Lond.* A **123**, 440–465.

HALL, K. C. 1996 Induced and profile power requirements for carangiform swimming. *J. Fluids Struct.*, submitted.

HALL, S. R., YANG, K. Y. & HALL, K. C. 1994 Helicopter rotor lift distributions for minimum induced power loss. *J. Aircraft* **31**, 837–845.

JONES, R. T. 1980 Wing flapping with minimum energy. *Aero. J.* **84**, 214–217.

KATZ, J. & PLOTKIN, A. 1991 *Low-Speed Aerodynamics: From Wing Theory to Panel Methods.* McGraw-Hill.

LAN, C. E. 1979 The unsteady quasi-vortex-lattice method with applications to animal propulsion. *J. Fluid Mech.* **93**, 747–765.

LIGHTHILL, M. J. 1970 Aquatic animal propulsion of high hydromechanical efficiency. *J. Fluid Mech.* **44**, 265–301.

MANGLER, K. W. 1951 Improper integrals in theoretical aerodynamics. *British ARC R & M* 2424.

PENNYCUICK, C. J. 1988 On the reconstruction of pterosaurs and their manner of flight, with notes on vortex wakes. *Biol. Rev.* **63**, 299–331.

PHLIPS, P. J., EAST, R. A. & PRATT, N. H. 1981 An unsteady lifting line theory of flapping wings with application to the forward flight of birds. *J. Fluid Mech.* **112**, 97–125.

RAYNER, J. M. V. 1979 A vortex theory of animal flight. Part 2. The forward flight of birds. *J. Fluid Mech.* **91**, 731–763.

RAYNER, J. M. V. 1991 Wake structure and force generation in avian flapping flight. In *Acta XX Congressus Internationalis Ornithologici* (ed. B. D. Bell), vol. 2, pp. 702–715.

RAYNER, J. M. V. 1993 On aerodynamics and the energetics of vertebrate flapping flight. In *Fluid Dynamics in Biology* (ed. A. Y. Cheer & C. P. van Dam). Contemporary Mathematics, vol. 141, pp. 351–400. American Mathematical Society.

RAYNER, J. M. V., JONES, G. & THOMAS, A. 1986 Vortex flow visualizations reveal change in upstroke function with flight speed in bats. *Nature* **321**, 162–164.

RIBNER, H. S. & FOSTER, S. P. 1990 Ideal efficiency of propellers: Theodorsen revisited. *J. Aircraft* **27**, 810–819.

SPEDDING, G. R. 1986 The wake of a jackdaw (*Corvus monedula*) in slow flight. *J. Exp. Biol.* **125**, 287–307.

SPEDDING, G. R. 1987 The wake of a kestrel (*Falco tinnunculus*) in flapping flight. *J. Exp. Biol.* **127**, 59–78.

SPEDDING, G. R., RAYNER, J. M. V. & PENNYCUICK, C. J. 1984 Momentum and energy in the wake of a pigeon (*Columba livia*) in slow flight. *J. Exp. Biol.* **111**, 81–102.

THEODORSEN, T. 1948 *Theory of Propellers.* McGraw-Hill.

TUCKER, V. A. 1968 Respiratory exchange and evaporative water loss in the flying budgerigar. *J. Exp. Biol.* **48**, 67–87.

TUCKER, V. A. 1972 Metabolism during flight in the laughing gull, *Larus atricilla. American J. Physiol.* **222**, 237–245.

TUCKER, V. A. 1973 Bird metabolism during flight: evaluation of a theory. *J. Exp. Biol.* **58**, 689–709.

WILMOTT, P. 1988 Unsteady lifting-line theory by the method of matched asymptotic expansions. *J. Fluid Mech.* **186**, 303–320.